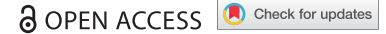




RESEARCH PAPER



A facile forward-genetic screen for *Arabidopsis* autophagy mutants reveals twenty-one loss-of-function mutations disrupting six ATG genes

Pierce G. Young ^{a*}, Michael J. Passalacqua^{a†}, Kevin Chappell^{a,b}, Roxanna J. Llinas^a, and Bonnie Bartel ^a

^aDepartment of Biosciences, Rice University, Houston, TX, USA; ^bDepartment of Biology, University of Mary Hardin-Baylor, Belton, TX, USA

ABSTRACT

Macroautophagy is a process through which eukaryotic cells degrade large substrates including organelles, protein aggregates, and invading pathogens. Over 40 autophagy-related (ATG) genes have been identified through forward-genetic screens in yeast. Although homology-based analyses have identified conserved ATG genes in plants, only a few *atg* mutants have emerged from forward-genetic screens in *Arabidopsis thaliana*. We developed a screen that consistently recovers *Arabidopsis atg* mutations by exploiting mutants with defective LON2/At5g47040, a protease implicated in peroxisomal quality control. *Arabidopsis lon2* mutants exhibit reduced responsiveness to the peroxisomally-metabolized auxin precursor indole-3-butyric acid (IBA), heightened degradation of several peroxisomal matrix proteins, and impaired processing of proteins harboring N-terminal peroxisomal targeting signals; these defects are ameliorated by preventing autophagy. We optimized a *lon2* suppressor screen to expedite recovery of additional *atg* mutants. After screening mutagenized *lon2-2* seedlings for restored IBA responsiveness, we evaluated stabilization and processing of peroxisomal proteins, levels of several ATG proteins, and levels of the selective autophagy receptor NBR1/At4g24690, which accumulates when autophagy is impaired. We recovered 21 alleles disrupting 6 ATG genes: *ATG2/At3g19190*, *ATG3/At5g61500*, *ATG5/At5g17290*, *ATG7/At5g45900*, *ATG16/At5g50230*, and *ATG18a/At3g62770*. Twenty alleles were novel, and 3 of the mutated genes lack T-DNA insertional alleles in publicly available repositories. We also demonstrate that an insertional *atg11/At4g30790* allele incompletely suppresses *lon2* defects. Finally, we show that NBR1 is not necessary for autophagy of *lon2* peroxisomes and that *NBR1* overexpression is not sufficient to trigger autophagy of seedling peroxisomes, indicating that *Arabidopsis* can use an NBR1-independent mechanism to target peroxisomes for autophagic degradation.

Abbreviations: ATG: autophagy-related; ATI: ATG8-interacting protein; Col-0: Columbia-0; DSK2: dominant suppressor of KAR2; EMS: ethyl methanesulfonate; GFP: green fluorescent protein; IAA: indole-3-acetic acid; IBA: indole-3-butyric acid; ICL: isocitrate lyase; MLS: malate synthase; NBR1: Next to BRCA1 gene 1; PEX: peroxin; PMDH: peroxisomal malate dehydrogenase; PTS: peroxisomal targeting signal; thiolase: 3-ketoacyl-CoA thiolase; UBA: ubiquitin-associated; WT: wild type

ARTICLE HISTORY

Received 2 March 2018
Revised 30 October 2018
Accepted 5 December 2018

KEYWORDS

LON2 protease; organelle quality control; pexophagy; peroxisome turnover; suppressor genetics

Introduction

Eukaryotes use macroautophagy, hereafter referred to as autophagy, to maintain cellular homeostasis during development and in response to environmental changes. This degradation process targets protein aggregates, pathogens, damaged or superfluous organelles, and other cellular components [1–6]. During autophagy, a double-membrane structure known as a phagophore surrounds and engulfs the fated cargo. Once enclosed, the outer membrane of the resulting double-membrane-bound autophagosome fuses with a lysosome (in metazoans) or vacuole (in plants and fungi) to deliver the cargo into the lysosome or vacuole lumen. The cargo is broken down, and constituent amino acids, lipids, and carbohydrates are returned to the cytosol, where these molecules can be recycled to synthesize new organelles and proteins.

In plants, autophagy promotes survival during starvation and harsh environmental conditions. Autophagy is upregulated in


plants during nutrient deprivation [7], and plants lacking autophagy are hypersensitive to carbon and nitrogen starvation [8], fungal infection [9], and various abiotic stresses, including heat stress [10], drought and salt stress [11], and oxidative stress [12]. Autophagy is also upregulated during seed maturation [13], suggesting a role during embryo development. Although autophagy is not required for plant survival in optimal growth conditions [8], plants lacking autophagy accumulate the selective autophagy receptor NBR1 [14] and certain peroxisomal proteins [15,16], suggesting that basal autophagy also contributes to general intracellular processes.

Nearly half of the over 40 identified autophagy-related (ATG) proteins are part of the core autophagy machinery that is conserved across kingdoms, including in the reference plant *Arabidopsis thaliana* [3–6]. These core ATG proteins can be grouped by the functions that they support. ATG1, ATG11, ATG13, and ATG101 are involved in initiating autophagosome

CONTACT Bonnie Bartel  bartel@rice.edu  Department of Biosciences, Rice University, MS-140, 6100 Main St., Houston, TX 77005 USA

*Present address: Department of Biochemistry and Biophysics, Texas A&M University, College Station, TX 77863

†Present address: Center for Cell and Gene Therapy, Baylor College of Medicine, Houston, TX 77030

 Supplemental data for this article can be accessed [here](#).

© 2019 The Author(s). Published by Informa UK Limited, trading as Taylor & Francis Group.

This is an Open Access article distributed under the terms of the Creative Commons Attribution-NonCommercial-NoDerivatives License (<http://creativecommons.org/licenses/by-nc-nd/4.0/>), which permits non-commercial re-use, distribution, and reproduction in any medium, provided the original work is properly cited, and is not altered, transformed, or built upon in any way.

formation [7,17,18]. ATG2, ATG6, ATG9, and ATG18 participate in phagophore expansion [18–24]. ATG8 is a ubiquitin-like protein that decorates the phagophore via conjugation to phosphatidylethanolamine [8,25,26], and this ATG8 lipidation requires ATG3, ATG4, ATG5, ATG7, ATG10, ATG12, and ATG16 [8,27–32].

A variety of receptors with differing cargo specificity mediate selective autophagy by controlling which substrates are engulfed by autophagosomes. Selective autophagy receptors link organelles, protein aggregates, or other cargo to the autophagy machinery by binding to both the fated cargo and ATG8 [33]. These receptors generally bind ATG8 via an ATG8-interacting motif with the consensus core sequence [W/Y/F]xx[L/I/V] with neighboring acidic (D or E) residues [33,34]. The ability to recognize not only specific types of organelles but also damaged or unnecessary organelles is paramount to maintaining cellular homeostasis, and the molecular mechanisms that enact various selective autophagy pathways continue to be unraveled.

Several selective autophagy receptors have been characterized [4,33]. For example, mammalian NBR1 and SQSTM1/p62 (sequestosome 1) bind both LC3/ATG8 and ubiquitin [33]. Plants encode NBR1 orthologs (known as Joka2 in tobacco), but plant orthologs of SQSTM1/p62 have not been identified [14,35]. *Arabidopsis nbr1* mutants display sensitivity to only a subset of the stressors to which *atg* mutants display sensitivity [10,36], suggesting that NBR1 acts as a selective autophagy receptor for a subset of autophagic cargos. For example, *Arabidopsis* NBR1 is implicated in clearing ubiquitinated protein aggregates following heat stress [10] and in limiting cauliflower mosaic virus infection by targeting virus particle-forming capsid proteins for autophagic degradation [37] but appears not to participate in autophagy of proteasomes [38]. Several plant-specific ATI (ATG8-interacting) proteins [39,40] are implicated in autophagy. For example, ATI1/At2g45980 plays a role in autophagy of plastids [41], and ATI3A/At1g17780 is implicated in autophagy of the endoplasmic reticulum (ER) [40]. Besides ATI proteins, *Arabidopsis* uses a ubiquitin receptor to target a transcription factor for autophagic degradation [42] and uses a proteasome subunit as a receptor for autophagy of proteasomes [38].

One target of autophagy is the peroxisome, an organelle that sequesters oxidative reactions. Most notably, peroxisomes house fatty acid β -oxidation, which converts fatty acids into acetyl-CoA and produces hydrogen peroxide (H_2O_2) as a byproduct [43]. Peroxisomes use various enzymes to detoxify H_2O_2 , including catalase [44], which is itself susceptible to oxidative damage by H_2O_2 [45]. Pexophagy, the selective autophagy of peroxisomes, contributes to peroxisome homeostasis in plants by degrading damaged or obsolete peroxisomes [46]. Pexophagy occurs at a higher basal rate than autophagy of other organelles in *Arabidopsis* seedlings, as evidenced by the higher relative accumulation of peroxisomal versus other organellar proteins in *atg5* mutants [15,47]. Moreover, *Arabidopsis atg* mutants accumulate peroxisomes [16] and nonfunctional, oxidized catalase [15,47], suggesting a role for pexophagy in maintaining peroxisome function. However, the molecular mechanisms by which plant cells recognize peroxisomes in need of turnover remain unclear.

In addition to quality control via pexophagy, plant cells regulate peroxisome homeostasis through the peroxisomal matrix protease LON2 [48–50]. Like *E. coli* Lon [51,52] and yeast Pln/peroxisomal Lon [53,54], LON2 is an AAA ATPase thought to act as both a chaperone and a protease that recovers misfolded proteins and degrades proteins that cannot be refolded; the chaperone function of LON2 is implicated in preventing pexophagy [50]. Dysfunctional LON2 results in enlarged peroxisomes and heightened pexophagy [48,50,55]. Notably, the peroxisomal glyoxylate cycle enzymes ICL (isocitrate lyase/At3g21720) and MLS (malate synthase/At5g03860) are degraded at wild-type rates when LON2 is disrupted, weakly stabilized when autophagy is disrupted, and strongly stabilized when both LON2 and autophagy are disrupted [48,50], implicating both LON2 and autophagy in ICL and MLS turnover. In contrast, the peroxisomal β -oxidation enzyme thiolase (3-ketoacyl-CoA thiolase/At2g33150) is destabilized in *lon2* mutants [49] but stabilized when autophagy or both LON2 and autophagy are disrupted [48,50], hinting that thiolase is primarily turned over via pexophagy.

We have previously recovered 1 *atg3*, 2 *atg2*, and 5 *atg7* alleles by screening for suppressors of *Arabidopsis lon2* mutants [48,56]. Peroxisomal β -oxidation converts the auxin precursor indole-3-butyric acid (IBA) to the active hormone indole-3-acetic acid (IAA) [57–59], and IBA treatment promotes abundant lateral root production [58,60] due to the IAA produced by metabolism of IBA. Unlike wild type, *lon2* scarcely forms lateral roots in response to IBA [49] because *lon2* peroxisomes are excessively degraded by pexophagy [48], decreasing peroxisome abundance and thereby presumably decreasing IBA-to-IAA conversion. Because screening for suppressors restoring *lon2* IBA responsiveness affords a homology-independent method to uncover autophagy components in *Arabidopsis* [48], we expanded the *lon2* suppressor screen. This effort yielded 21 alleles of 6 ATG genes, including 1 *atg3*, 2 *atg2*, 2 *atg5*, 2 *atg18a*, 3 *atg16*, and 11 *atg7* mutants. We did not recover *atg11* or *nbr1* mutants in our screen, but using reverse genetics, we demonstrated that loss of *ATG11* incompletely suppresses *lon2* phenotypes and that the selective autophagy receptor NBR1 is neither necessary for pexophagy in the *lon2* mutant nor sufficient for stimulating pexophagy when overexpressed in *Arabidopsis* seedlings.

Results

Forward-genetic screening strategy for *Arabidopsis* autophagy mutants

We used a 4-step strategy (Figure 1) to recover 21 mutants carrying mutations in 6 different *Arabidopsis* ATG genes (Table 1). First, to identify potential *atg* mutants, we screened approximately 500,000 8-day-old *lon2-2* M_2 seedlings from 104 mutagenized pools for the presence of lateral roots on medium containing 8 μ M IBA (Figure 1(a)). Unlike wild-type seedlings, *lon2* seedlings fail to form abundant lateral roots in response to IBA [49], and preventing autophagy in *lon2* mutants suppresses this phenotype [48].

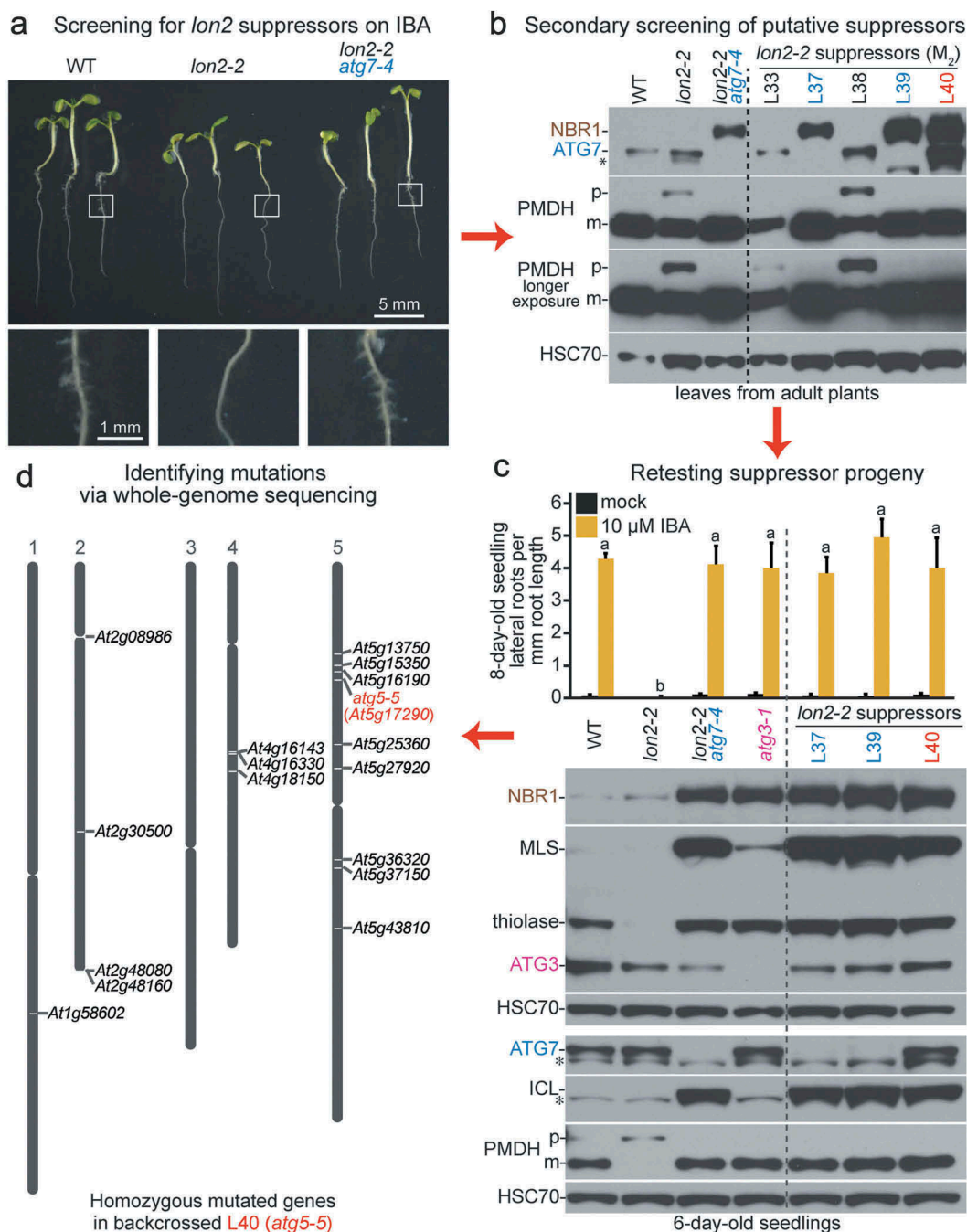


Figure 1. Four-step strategy for isolating *Arabidopsis* autophagy-defective mutants. (a) Initial screening for *lon2* suppressors. *lon2* forms few lateral roots in response to IBA; putative suppressors that formed lateral roots in the presence of IBA similar to wild-type and *lon2-2 atg7-4* were moved to soil for propagation. Top panel: wild-type (WT), *lon2-2*, and *lon2-2 atg7-4* seedlings were grown on media containing 8 μ M IBA and imaged at 8 days; scale bar: 5 mm. Bottom row: magnified images of roots outlined in the top panel showing lateral roots, which are absent in *lon2-2*; scale bar: 1 mm. (b) Secondary screening of putative suppressors. Leaf extracts from approximately 30-day-old adult controls (left of dashed line) or M_2 putative suppressor plants (right of dashed line) were processed for immunoblotting with antibodies to the indicated proteins. NBR1 is a selective autophagy receptor that accumulates in *atg* mutants [14]. PMDH is synthesized as a precursor (p) that is processed to a mature form (m) in the peroxisome. HSC70 is a loading control. The asterisk indicates a protein cross-reacting with the ATG7 antibody. (c) Retesting progeny of putative suppressors that displayed restored PTS2 processing in the M_2 generation. Top: lateral root density of 8-day-old controls (left of dashed line) or M_3 or M_4 suppressor seedlings (right of dashed line) grown without or with IBA. Error bars show standard deviations ($n = 8$). Statistically significant ($P < 0.0001$) differences determined by one-way ANOVA are depicted by different letters above the bars. Bottom: extracts from 6-day-old controls (left of dashed line) or M_3 or M_4 suppressor seedlings (right of dashed line) were processed for immunoblotting. Membranes from duplicate gels were serially probed with antibodies to the indicated proteins to obtain the top 3 and bottom 4 panels. MLS, thiolase, and ICL are peroxisomal proteins that are stabilized when both LON2 and autophagy are defective [48]. Asterisks indicate proteins cross-reacting with the ATG7 or ICL antibodies. (d) Identifying mutations via whole-genome sequencing. The L40 suppressor was backcrossed to the original *lon2-2* line, IBA-sensitive F_2 seedlings were selected, and genomic DNA from pooled F_3 seedlings was sequenced. Homozygous single-nucleotide polymorphisms consistent with EMS mutagenesis (G/C to A/T transitions) and causing nonsynonymous mutations in coding regions, altering splice sites, or occurring in introns or untranslated regions are indicated by locus identifiers and displayed to the right of the 5 *Arabidopsis* chromosomes using The *Arabidopsis* Information Resource Chromosome Map Tool.

Table 1. ATG Mutant alleles recovered as *lon2-2* suppressors in this work.

Gene (accession number)	Protein function	Allele	Alias ¹	Nucleotide change	Protein or transcript change
<i>ATG2</i> (<i>At3g19190</i>)	Phagophore expansion	<i>atg2-6</i>	L60	g6271a	Intron 6 splice-acceptor site
		<i>atg2-7</i>	L78, L79	g795a	W90Stop
<i>ATG3</i> (<i>At5g61500</i>)	ATG8 lipidation (E2-like)	<i>atg3-2</i>	L13, L14, L15, L16	g1613a	Intron 5 splice-acceptor site
<i>ATG5</i> (<i>At5g17290</i>)	ATG8 lipidation (E3-like)	<i>atg5-5</i>	L40, L41	g1387a	Intron 4 splice-acceptor site
		<i>atg5-6</i>	L43, L44, L45	g2615a	E323K
<i>ATG7</i> (<i>At5g45900</i>)	ATG8 lipidation (E1-like)	<i>atg7-6²</i>	L61	g1648a	W344Stop
		<i>atg7-10</i>	L21, L23, L24, L27	g140a	Intron 1 splice-donor site
		<i>atg7-11</i>	L160	g552a	G91E
		<i>atg7-12</i>	L37, L46	g715a	Intron 2 splice-acceptor site
		<i>atg7-13</i>	L17, L18	g721a	W1195Stop
		<i>atg7-14</i>	L123	g940a	W192Stop
		<i>atg7-15</i>	L39	g1454a	W307Stop
		<i>atg7-16</i>	L66	g2269a	Intron 7 splice-acceptor site
		<i>atg7-17</i>	L20, L25	g2394a	G535D
		<i>atg7-19</i>	L71	c2562t	T559I
		<i>atg7-21</i>	L92, L93, L96, L97	c2848t	Q629Stop
		<i>ATG16</i> (<i>At5g50230</i>)	ATG8 lipidation (membrane tethering)	<i>atg16-1</i>	L65
<i>atg16-2</i>	L68			g650a; g760a	Intron 2 splice-acceptor site; R80K
<i>atg16-3</i>	L53			c810t	Q97Stop
<i>ATG18a</i> (<i>At3g62770</i>)	Phagophore expansion	<i>atg18a-3</i>	L1	c463t	Q1555Stop
		<i>atg18a-4</i>	L154	g1921a	W3645Stop

¹In all but one case, multiple isolates of allelic mutations were from the same M₂ pool, indicating that the isolates were likely siblings. The exception was *atg7-12*, which was isolated from 2 independent pools.

²*atg7-6* was independently isolated in a pilot *lon2-2* suppressor screen [48].

Second, to eliminate false positives and mutants with elevated auxin levels or responsiveness, we moved seedlings with lateral roots to soil and collected leaf tissue from approximately 30-day-old plants for immunoblot analysis. We used antibodies recognizing NBR1, PMDH (peroxisomal malate dehydrogenase/*At5g09660*), and ATG7 to identify suppressors with impaired autophagy and improved peroxisome function (Figure 1(b)). The selective autophagy receptor NBR1 is degraded at a basal rate via autophagy and accumulates when autophagy is impaired [14]. PMDH is synthesized as precursor containing an N-terminal peroxisomal-targeting signal 2 (PTS2) that is removed following peroxisomal import. The incomplete PTS2 processing in *lon2* plants [49] presumably stems from elevated pexophagy, which reduces the number of peroxisomes; preventing autophagy restores PMDH processing in *lon2-2* by increasing the number of import-competent peroxisomes [48]. M₂ plants with elevated NBR1 levels and restored PMDH processing were prioritized as likely *atg* mutants, and plants with decreased ATG7 levels were candidate *atg7* mutants (Figure 1(b)).

Third, to confirm *lon2-2* suppression, we collected M₃ or M₄ progeny of putative suppressors; retested IBA responsiveness; and examined thiolase, MLS or ICL, and ATG3 levels in 6-day-old seedlings (Figure 1(c)). Thiolase is a peroxisomal enzyme that is destabilized in *lon2-2* seedlings [49] and stabilized in *lon2-2 atg* mutants [48]. Similarly, the peroxisomal enzymes ICL and MLS are stabilized in *lon2-2 atg* double mutants [48]. Mutants with elevated thiolase and ICL or MLS were prioritized as likely *atg* mutants, and plants with decreased ATG3 levels were candidate *atg3* mutants.

Fourth, we used DNA sequencing to identify causal lesions. We sequenced *ATG7* or *ATG3* in suppressors with decreased levels of the respective proteins and prepared DNA for whole-genome sequencing for the remaining suppressors (Figure 1(d)).

New *atg7* alleles recovered as *lon2* suppressors

ATG7, which encodes an E1-like enzyme involved in ATG8 lipidation [8], was the most commonly mutated gene among our *lon2* suppressors (Figure 2; Table 1). Most of these suppressors were initially identified as *atg7* mutants due to low or undetectable ATG7 levels (Figure 2(c)). *atg7-19* displayed near wild-type ATG7 levels and was identified by whole-genome sequencing (Fig. S1B). We identified 5 nonsense mutations (*atg7-6*, *atg7-13*, *atg7-14*, *atg7-15*, and *atg7-21*), 3 splice-site mutations (*atg7-10*, *atg7-12*, and *atg7-16*), and 3 missense mutations (*atg7-11*, *atg7-17*, and *atg7-19*) (Figure 2(a)). The 3 missense alleles alter residues that are conserved in ATG7 enzymes from *Arabidopsis*, humans, fruit flies, and budding yeast (Fig. S2). Interestingly, *atg7-19* alters the conserved Thr559 residue immediately following the ATG7 active site Cys558 residue (Figure 2(a); Fig. S2). Although primarily novel *atg7* alleles were recovered, a few duplicate alleles were isolated. The *atg7-12* splice-site allele was found in 2 independent M₂ pools, and an *atg7-6* nonsense allele was previously recovered in our pilot *lon2* suppressor screen [48]. Moreover, the nonsense allele *atg7-13* harbors a mutation in a different nucleotide of the same codon as the previously published allele *atg7-5* [48]; although non-allelic, both of these mutations result in

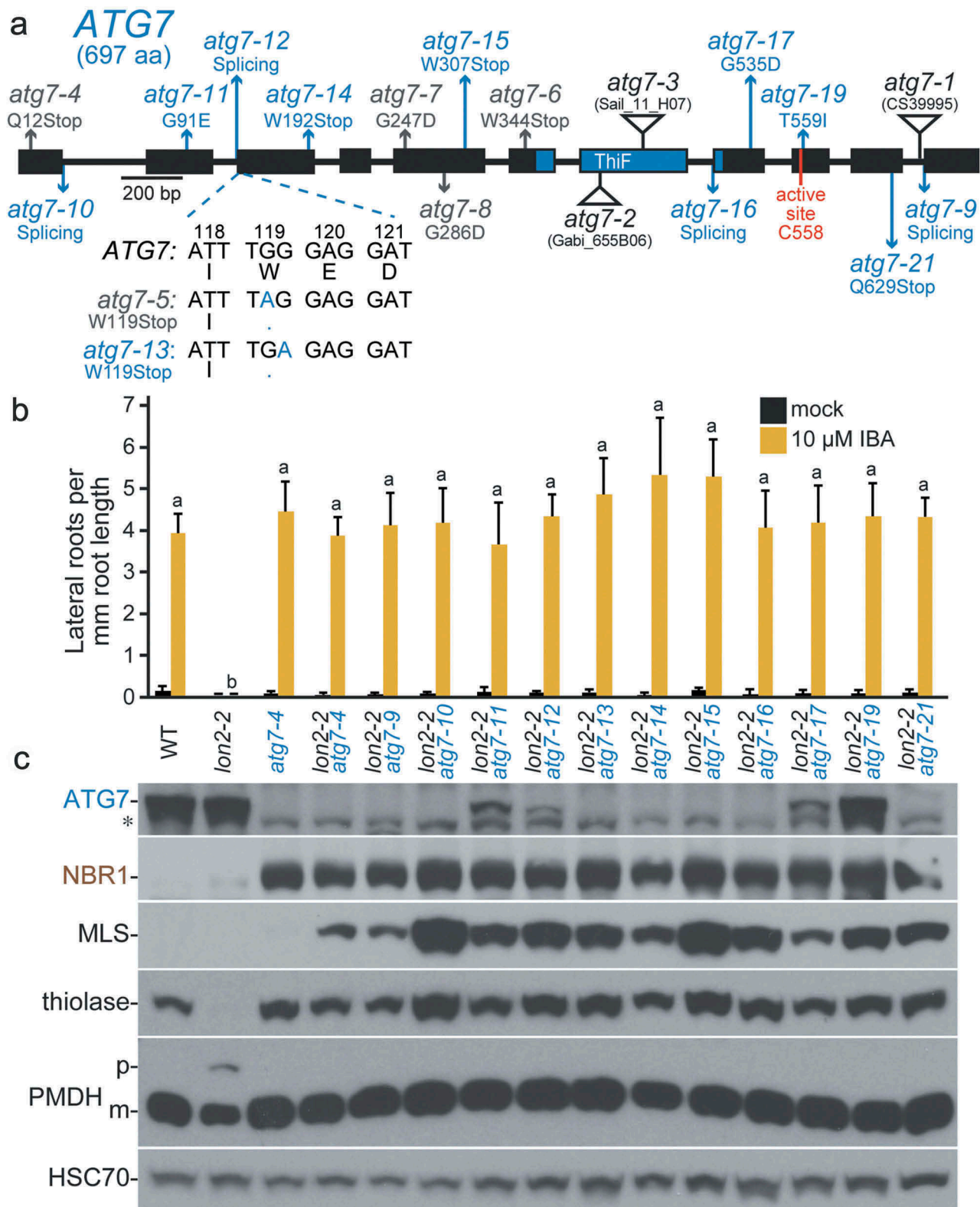


Figure 2. Numerous novel *atg7* alleles recovered as *lon2* suppressors. (a) Diagram of the *ATG7* gene. Boxes and lines represent protein-coding regions and introns, respectively. The ThiF-like adenylation domain and active-site Cys residue are indicated. The positions of new *atg7* mutations identified as *lon2* suppressors are in blue; previously described EMS-derived *lon2* suppressors [48] are in gray, and T-DNA insertion alleles [8,9,61] are indicated by triangles. *atg7-9* is an unpublished allele (alias 8–30) from the pilot *lon2-2* suppressor screen [48] that carries a g2959a mutation in the intron 10 splice acceptor site. The sequence of the *atg7-13* nonsense allele compared to *atg7-5* and wild-type *ATG7* is shown below the gene diagram. aa, amino acids. (b) Lateral root density of 8-day-old wild type (WT), *lon2-2*, *atg7-4*, and *lon2-2 atg7* seedlings grown without or with IBA. Error bars show standard deviations ($n = 8$). Statistically significant ($P < 0.0001$) differences determined by one-way ANOVA are depicted by different letters above the bars. (c) Extracts from 6-day-old seedlings were processed for immunoblotting with antibodies to the indicated proteins. The asterisk indicates a protein cross-reacting with the *ATG7* antibody.

the same protein alteration (W119Stop; Figure 2(a)). All of the *atg7* mutants restored IBA responsiveness to *lon2-2* (Figure 2(b)) and displayed the characteristic immunoblot phenotypes of 6-day-old *lon2-2 atg* double mutants: accumulated NBR1, stabilized MLS and thiolase, and restored PTS2 processing (Figure 2(c)). The early nonsense and splice-site mutations are expected to encode null alleles, and, indeed, we did not detect ATG7 protein in most of these mutants (Figure 2(c)). The 3 missense alleles (*atg7-11*, *atg7-17*, and *atg7-19*) accumulated detectable ATG7 protein (Figure 2(c)) and could therefore retain partial function, but these mutants nevertheless suppressed *lon2-2* as well as the nonsense and splice-site alleles (Figure 2(b, c)).

New *atg3*, *atg5*, and *atg16* alleles recovered as *lon2* suppressors

In addition to ATG7, we isolated novel alleles of 3 other genes involved in ATG8 lipidation. We identified the *atg3-2* splice-site mutation by sequencing ATG3, which encodes an E2-like enzyme that conjugates ATG8 to phosphatidylethanolamine [32], from a mutant that lacked detectable ATG3 protein (Figure 3(c)).

We recovered 2 mutations in ATG5, which encodes a protein with 2 ubiquitin-like domains that is conjugated by the ubiquitin-like protein ATG12 to act as an E3-like enzyme in ATG8 lipidation [29,31,62]. We used whole-genome sequencing to identify the *atg5-5* splice-site mutation (Figure 1(d), 3(a)) and the *atg5-6* missense mutation (Figure 3(a), Fig. S1A), which altered a conserved acidic residue (Glu323) in the second ubiquitin-like domain to a Lys residue (Fig. S3). We did not detect ATG5 protein in either of these mutants (Figure 3(c)).

We recovered 3 mutations in ATG16, which in yeast encodes a protein that tethers the ATG12–ATG5 conjugate to the membrane to allow ATG8 lipidation and autophagosome formation [31]. Whole-genome sequencing revealed that *atg16-1* and *atg16-3* harbored nonsense mutations (W47Stop and Q97Stop, respectively) and that *atg16-2* harbored both a splice-site mutation and a nearby missense mutation (R80K) (Figure 3(a), Fig. S1C to E). We surmise that the *atg16-2* splice site mutation is causal because it is expected to prevent full-length ATG16 accumulation and is 5' of the missense mutation.

All of the *atg3*, *atg5*, and *atg16* alleles similarly restored *lon2-2* IBA responsiveness (Figure 3(b)) and displayed the characteristic immunoblot phenotypes (Figure 3(c)) of other *lon2-2 atg* double mutant seedlings (e.g., Figure 1(c)).

Because the roles of ATG3 and ATG16 have not been confirmed in plants, we began this analysis by comparing ATG8 levels in an allele of each *atg* mutant in a wild-type *LON2* background. As previously reported [29], ATG8 levels were elevated in *atg5* and *atg7* mutants (Figure 3(d)). We found similarly elevated ATG8 levels in our *atg3* and *atg16* alleles (Figure 3(d)), which is consistent with the possibility that autophagy is impaired in these mutants.

New *atg2* alleles recovered as *lon2* suppressors

We used whole-genome sequencing to identify 2 mutations in ATG2 (Figure 4(a, b), Fig. S4), which encodes a protein involved in phagophore expansion. Both *atg2* mutants fully restored IBA responsiveness to *lon2-2* (Figure 4(d)) and displayed the characteristic immunoblot phenotypes (Figure 4(e)) of other *lon2-2 atg* seedlings (Figure 1(c), 2(c), 3(c)). Moreover, *atg2-6* displayed elevated ATG8 levels (Figure 3(d)). The *atg2-7* early nonsense mutation (W90Stop, Figure 4(b)) is expected to prevent ATG2 accumulation. The *atg2-6* mutation appeared in the middle of a cluster of mutations on chromosome 3 (Figure 4(a)) identified by sequencing backcrossed seedlings. However, the mutation was in intron 6 according to the primary prediction of Araport 11, the latest *A. thaliana* genome annotation. Araport 11 also predicts 2 ATG2 splice variants that would result in *atg2-6* interrupting a splice-acceptor site. Indeed, the region of the intron following the mutated nucleotide can be translated in frame with exon 7 and lacks stop codons (Figure 4(b)). Moreover, aligning predicted ATG2 proteins of other Brassicaceae family members revealed that this region of the predicted *Arabidopsis* intron 6 is conserved and exonic in other Brassicaceae ATG2 orthologs (Figure 4(b)), supporting the conclusion that the mutation in *atg2-6* disrupts a splice site in *A. thaliana* and suggesting that the 'alternative' splice variant encodes an ATG2 isoform that is essential for autophagy. Although the predicted splicing of *A. lyrata* ATG2 matched that of the *A. thaliana* ATG2 predicted by Araport 11, the *A. lyrata* genome was assembled based in part on alignment with *A. thaliana* [63], meaning that annotation errors in the *A. thaliana* genome may have been propagated to *A. lyrata*. Based on the whole-genome sequencing and Brassicaceae ATG2 alignment, we considered *atg2-6* as a splice-site mutation and the causal suppressor lesion.

New *atg18a* alleles recovered as *lon2* suppressors

Like ATG2, ATG18a is involved in phagophore expansion. We used whole-genome sequencing to identify the *atg18a-3* and *atg18a-4* nonsense mutations (Q155Stop, W364Stop, Figure 4(c), Fig. S5). *atg18a-3* and *atg18a-4* fully restored IBA responsiveness to *lon2-2* (Figure 4(d)) and displayed the characteristic immunoblot phenotypes of other *lon2-2 atg* seedlings (Figure 4(e)). Moreover, *atg18a-3* seedlings displayed similarly elevated ATG8 levels as other *atg* null alleles (Figure 3(d)).

To further probe the importance of ATG18a in pexophagy, we backcrossed *lon2-2 atg18a-3* to remove *lon2-2* and other unlinked mutations and examined *atg18a-3* seedlings constitutively expressing GFP carrying a peroxisomal targeting signal (GFP-PTS1) [66] using confocal microscopy. *atg7* and *atg5* mutants accumulate peroxisomes in hypocotyls of developing seedlings [16], and *atg18a* mutants display clusters of oxidized peroxisomes in mesophyll cells [15]. We observed increased peroxisome abundance relative to wild type in *atg18a-3* cotyledon epidermal cells, cotyledon mesophyll cells, and hypocotyl cells in 4- to 7-day-old seedlings (Figure 5), confirming that ATG18a promotes pexophagy during seedling development.

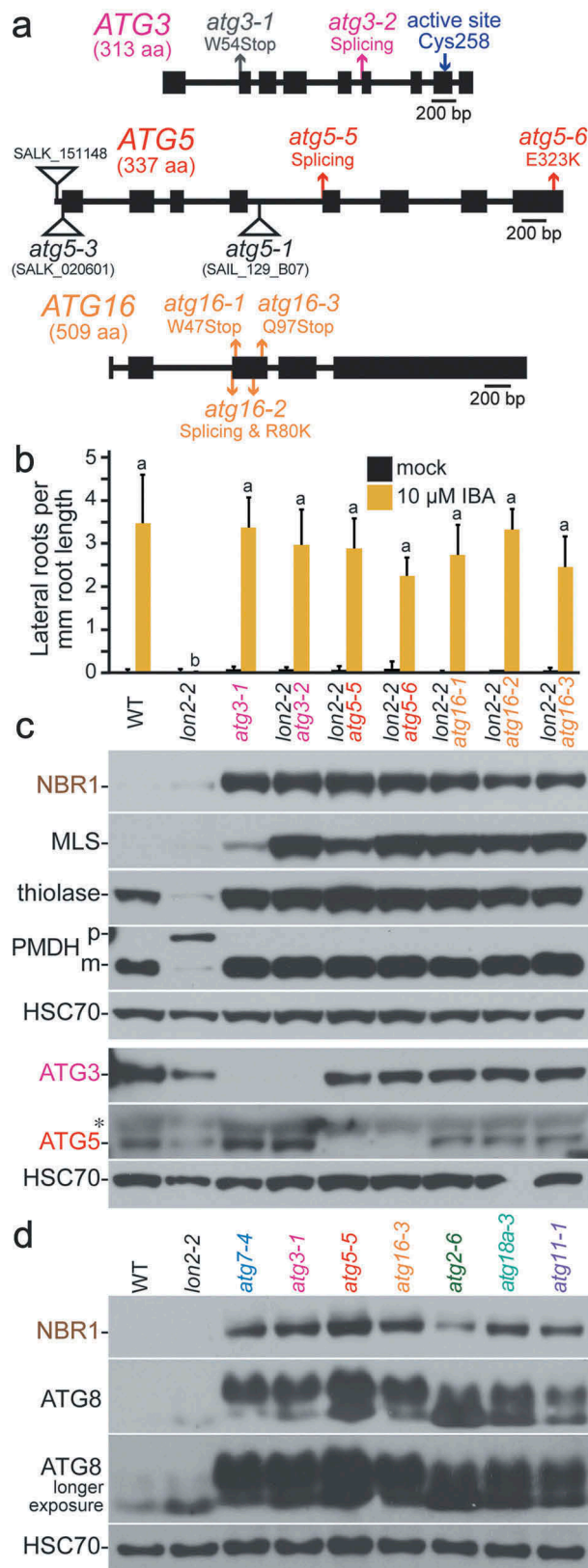


Figure 3. Novel *atg3*, *atg5*, and *atg16* alleles recovered as *lon2* suppressors. (a) Diagrams of the *ATG3*, *ATG5*, and *ATG16* genes. Boxes and lines represent protein-coding regions and introns, respectively. The positions of new *atg3*, *atg5*, and *atg16* mutations identified as *lon2* suppressors are shown in pink, red, and orange, respectively; the previously described *atg3-1* EMS-derived *lon2* suppressor [48] is in gray, and T-DNA insertion alleles [29,72,73] are indicated by triangles. aa, amino acids. (b) Lateral root density of 8-day-old wild type (WT), *lon2-2*, *atg3-1*, *lon2-2 atg3-2*, *lon2-2 atg5*, and *lon2-2 atg16* seedlings grown without or with IBA. Error bars show standard deviations ($n = 8$). Statistically significant ($P < 0.0001$) differences determined by one-way ANOVA are depicted by different letters above the bars. (c) Extracts from 6-day-old seedlings were processed for immunoblotting. Membranes from duplicate gels were serially probed with antibodies to the indicated proteins to obtain the top 5 and bottom 3 panels. The asterisk indicates a protein cross-reacting with the ATG5 antibody. (d) Extracts from 6-day-old seedlings were processed for immunoblotting and serially probed with antibodies to NBR1, ATG8A, and HSC70. ATG8 is lipidated and encoded by multiple genes in *Arabidopsis*.

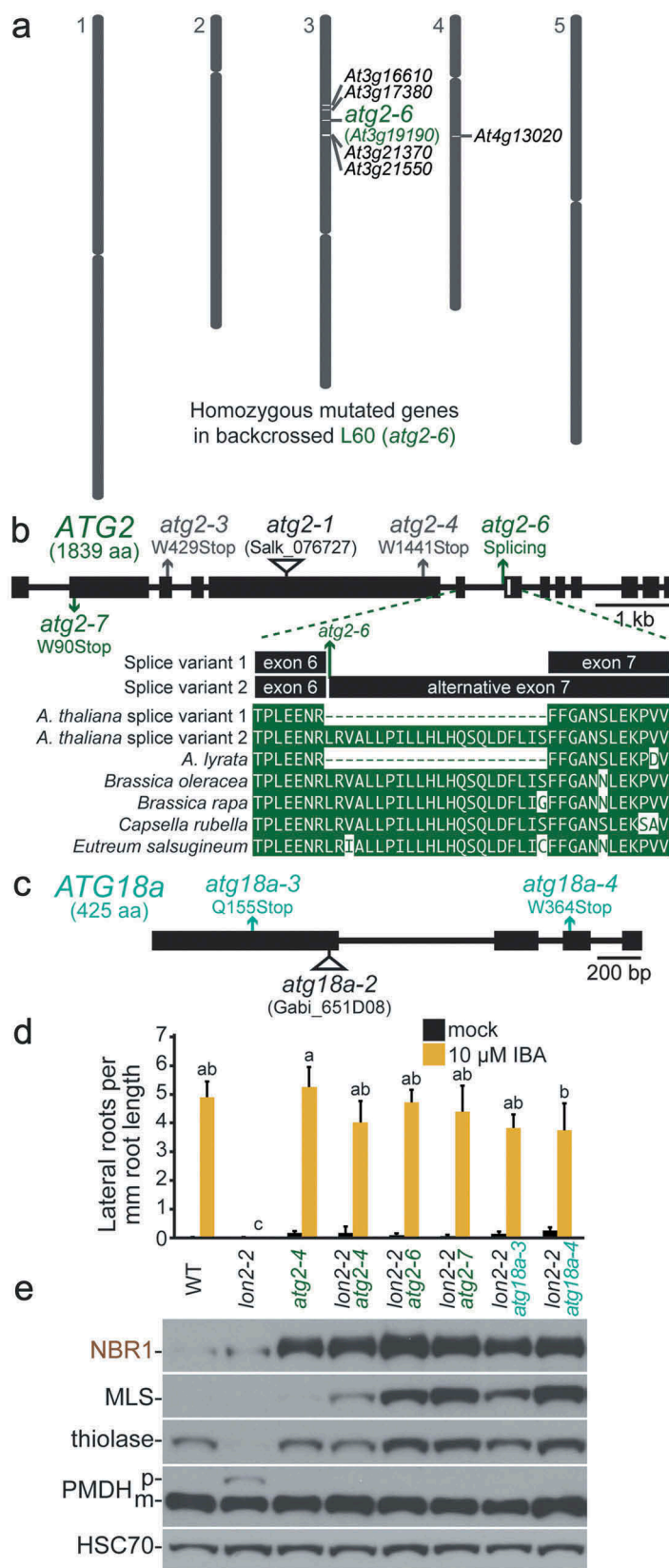


Figure 4. Novel *atg2* and *atg18a* alleles recovered as *lon2* suppressors. (a) The L60 suppressor was backcrossed to the original *lon2-2* line, and genomic DNA from pooled IBA-sensitive F₂ seedlings was sequenced and analyzed as in the legend to Figure 1(d). (b) *ATG2* gene diagram with boxes and lines representing protein-coding regions and introns, respectively. The positions of new *atg2* mutations identified as *lon2* suppressors are shown in green, previously described EMS-derived *lon2* suppressors [48] are in gray, and a T-DNA insertion allele [64] is indicated by a triangle. The partial alignment shows predicted Brassicaceae *ATG2* proteins, including 2 *A. thaliana* *ATG2* splice variants predicted by the latest genome annotation (Araport 11); the alternative *ATG2* splice variant is interrupted by the *atg2-6* mutation. aa, amino acids. (c) *ATG18a* gene diagram showing *atg18a* mutations identified as *lon2* suppressors (teal) and a previously described T-DNA insertion allele [65] (triangle). (d) Lateral root density of 8-day-old wild type (WT), *lon2-2*, *atg2-4*, *lon2-2 atg2*, and *lon2-2 atg18a* seedlings grown without or with IBA. Error bars show standard deviations (n = 8). Statistically significant (P < 0.0001) differences determined by one-way ANOVA are depicted by different letters above the bars. (e) Extracts from 6-day-old seedlings were processed for immunoblotting with antibodies to the indicated proteins.

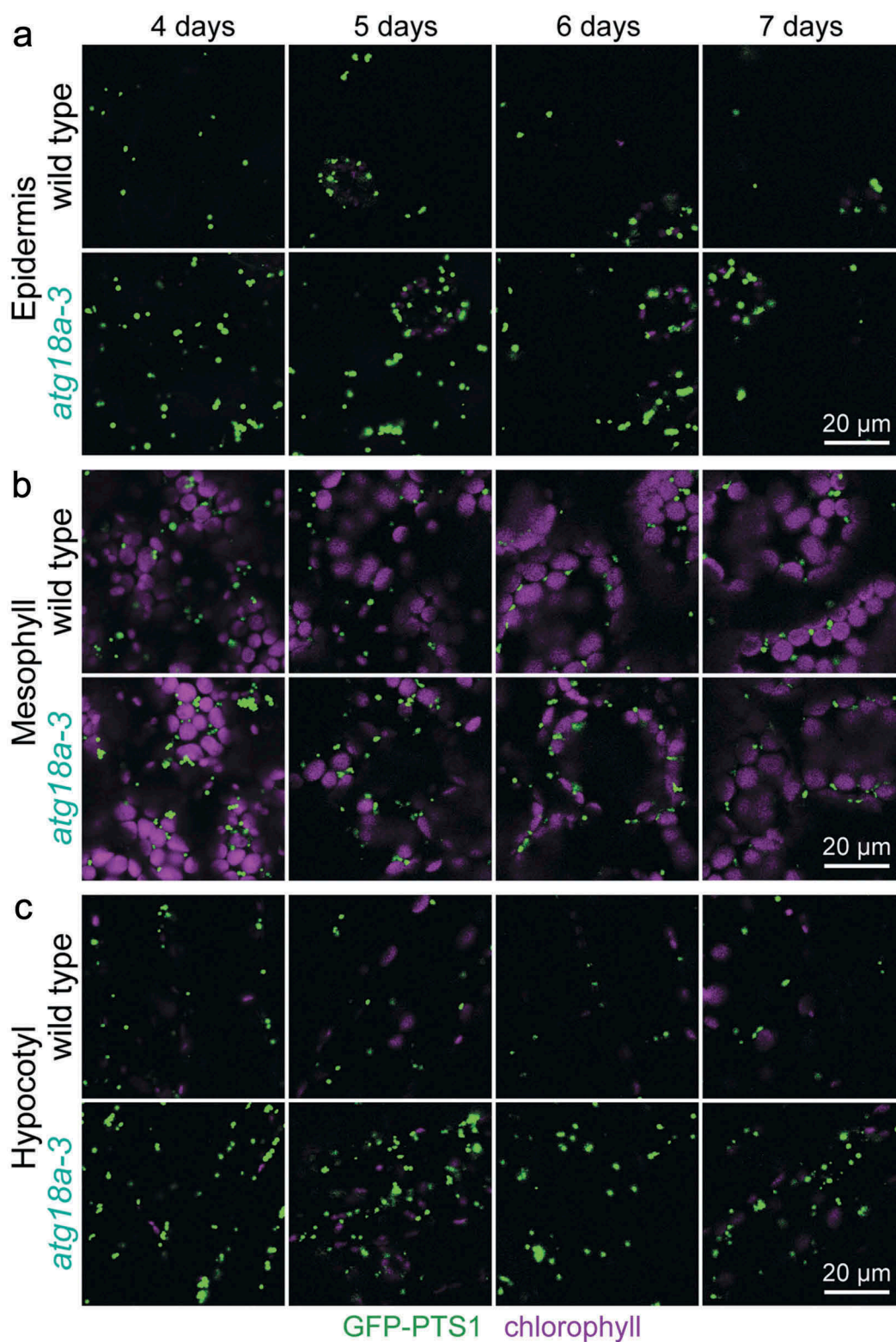


Figure 5. Increased peroxisome abundance in *atg18a-3* seedlings. (a) Cotyledon epidermal cells, (b) cotyledon mesophyll cells, and (c) hypocotyl cells in light-grown 4-, 5-, 6-, and 7-day-old wild-type and twice backcrossed *atg18a-3* seedlings expressing the peroxisomal matrix marker GFP-PTS1 were imaged for GFP fluorescence (green) and chlorophyll autofluorescence (magenta) using confocal microscopy. Scale bars: 20 μ m.

Loss of ATG11 partially suppresses *lon2* defects

Although *ATG11* functions in *Arabidopsis* autophagy [17,18], no *atg11* mutants emerged from our *lon2-2* suppressor screen. To test the importance of *ATG11* for *lon2*-related pexophagy,

we crossed the *atg11-1* T-DNA insertional allele (Figure 6(a)) [17] to *lon2-2*. Although the *lon2-2* PTS2-processing defect was fully suppressed in *lon2-2 atg11-1* (Figure 6(c)), *atg11-1* only partially suppressed *lon2-2* IBA resistance (Figure 6(b)),

thiolase was only partially stabilized in *lon2-2 atg11-1* (Figure 6(c)), and MLS was not stabilized (Figure 6(c)). This incomplete suppression suggested that some pexophagy still occurs in *atg11-1*. Additionally, ATG8 was only moderately elevated in *atg11-1* (Figure 3(d)), and NBR1 accumulated to intermediate levels in both *atg11-1* and *lon2-2 atg11-1* (Figure 6(c)), consistent with only partially disrupted autophagy.

NBR1 is not necessary for pexophagy of *lon2* peroxisomes

NBR1 is a selective autophagy receptor in *Arabidopsis* [10,14,36] and is necessary and sufficient for pexophagy in mammals [67], but no *nbr1* mutants emerged from our screen for *lon2-2* suppressors. To test the necessity of NBR1 for *Arabidopsis* pexophagy, we obtained T-DNA insertional alleles of *nbr1* (Figure 7(a)). These T-DNA insertions dramatically decreased full-length NBR1 protein accumulation (Figure 7(c)); however, the anti-NBR1 antibody was generated to the C-terminal UBA domain [14] and would not detect any N-terminal fragments of the protein that might accumulate in the mutants. Because intronic T-DNAs are sometimes removed by splicing [68,69], we characterized both intronic (*nbr1-1*) and exonic (*nbr1-4*) insertional mutants of *NBR1* in combination with *lon2-2*. Both *lon2 nbr1* double mutants resembled *lon2-2* and did not form lateral roots in response to IBA (Figure 7(b)). Moreover, neither *nbr1* allele stabilized MLS or thiolase or ameliorated the PTS2-processing defects of *lon2* (Figure 7(c)). This lack of suppression suggested that NBR1 is dispensable for pexophagy in *lon2*. Because *atg18a-3* accumulated peroxisomes (Figure 5), we also visualized *nbr1-4* expressing the peroxisomal marker GFP-PTS1 to evaluate peroxisome abundance. Unlike *atg18a-3*, peroxisome abundance in hypocotyls of 6-day-old *nbr1-4* seedlings resembled wild type (Figure 7(d)). The failure of *nbr1-4* mutants to accumulate excess peroxisomes suggested that NBR1 is not necessary for peroxisome turnover under our standard growth conditions.

If excess NBR1 was sufficient to induce pexophagy, then we would expect that overexpressing *NBR1* would stimulate pexophagy, as is observed in mammalian cells [67], and phenocopy *lon2*. We drove untagged, HA-tagged, and YFP-tagged *NBR1* from the constitutive cauliflower mosaic virus 35S promoter. Despite elevated NBR1 levels (Figure 7(e)), these lines resembled wild type in lateral root formation (Figure 7(b)), PTS2 processing (Figure 7(e)), and thiolase stability (Figure 7(e)). This failure of excess NBR1 to potentiate seedling pexophagy indicates that NBR1 is not limiting for pexophagy in *Arabidopsis*, which is consistent with the possibility that NBR1 is not a pexophagy receptor in *Arabidopsis* seedlings.

Discussion

A facile screen for *Arabidopsis atg* mutants

Screening for *lon2-2* suppressors revealed 21 alleles (20 novel alleles) in 6 *ATG* genes (Table 1), providing new mutants for investigating autophagy in *Arabidopsis*. A pilot *lon2-2* suppressor screen has uncovered *atg2*, *atg3*, and *atg7* mutants

[48], and the expanded screen described here uncovered additional alleles of these genes plus *atg5*, *atg16*, and *atg18a* mutants. In contrast to these *lon2* suppressor screens, a single *atg2* allele emerged from a forward-genetic screen for plants with enhanced cell death in response to fungal infection [22], a single *atg2* allele has emerged from a hydroxyurea-resistance screen [70] that primarily recovers *cat2* (*catalase/At4g35090*) mutants [71], and 2 *atg2* alleles along with single *atg7* and *atg18a* mutants have been recovered from a microscopy-based screen for aggregated peroxisomes [15]. The *lon2-2* suppressor screen combines high throughput with specificity and is the only forward-genetic screen to report *atg3*, *atg5*, or *atg16* mutants. Although *atg5* T-DNA insertional mutants have been characterized [29,72,73], no *Arabidopsis atg3* or *atg16* mutants have been reported aside from those arising from *lon2-2* suppressor screens described here and previously [48], and these alleles will be useful for future studies to determine whether *ATG3* and *ATG16* function similarly in *Arabidopsis* as in other organisms. Moreover, our *atg7* missense alleles (Figure 2(a), Fig. S2) may inform *ATG7* structure-function studies.

Roughly half (11 of 21) of the *lon2-2* suppressors harbored a mutation in *ATG7* (Table 1); the reason for this abundance of *atg7* mutants is mysterious. When adding the *atg7* alleles identified in our pilot screen [48], 16 of 29 *lon2-2* suppressors were *atg7* mutants, and *atg7-6* was independently isolated in both iterations of the screen (Table 1) [48]. Although *ATG7* encodes a large protein (697 amino acids), *ATG2* and *ATG11* encode larger proteins (1861 and 1148 amino acids, respectively) and thus would seem to be more likely mutagenic targets. However, our combined screening recovered only 4 *atg2* and no *atg11* mutants. Moreover, *ATG2* has 12 introns compared to 10 introns in *ATG7*, suggesting that *ATG2* would present more opportunities than *ATG7* for mutations in splice sites in addition to coding regions. The frequency of *atg7* mutants recovered in this screen might be explained by the structure and function of the *ATG7* protein. As an E1-like enzyme, *ATG7* activates both *ATG8* and *ATG12* and coordinates transfer to their respective E2-like enzymes, *ATG3* and *ATG10* [32,74–76]. *ATG7* is the interaction hub among these proteins, requiring precise spatial arrangement [32,74–77], so it is tempting to speculate that *ATG7* might be more susceptible to functional perturbation via missense mutations than other *ATG* proteins. Indeed, 5 of the 16 *atg7* mutants identified as *lon2-2* suppressors (*atg7-7*, *atg7-8*, *atg7-11*, *atg7-17*, and *atg7-19*; Figure 2(a), Fig. S2) harbor missense mutations whereas our only non-*atg7 lon2-2* suppressor to harbor an *atg* missense mutation is *atg5-6* (Figure 3(a), Fig. S3). However, fewer mutations in other *ATG* genes were recovered, hindering comparison of the relative proportions of null versus missense alleles; further screening might recover missense alleles of other *ATG* genes. Moreover, even discounting missense mutations, 11 of our *atg7* mutants harbor nonsense or splice-site mutations, which still exceeds the number of alleles recovered for any other *ATG* gene (Table 1), indicating that the explanation for the apparent bias towards *atg7* mutants may exist beyond the structure or function of *ATG7*. Perhaps the *ATG7* locus is more accessible to EMS mutagenesis than other *ATG* genes.

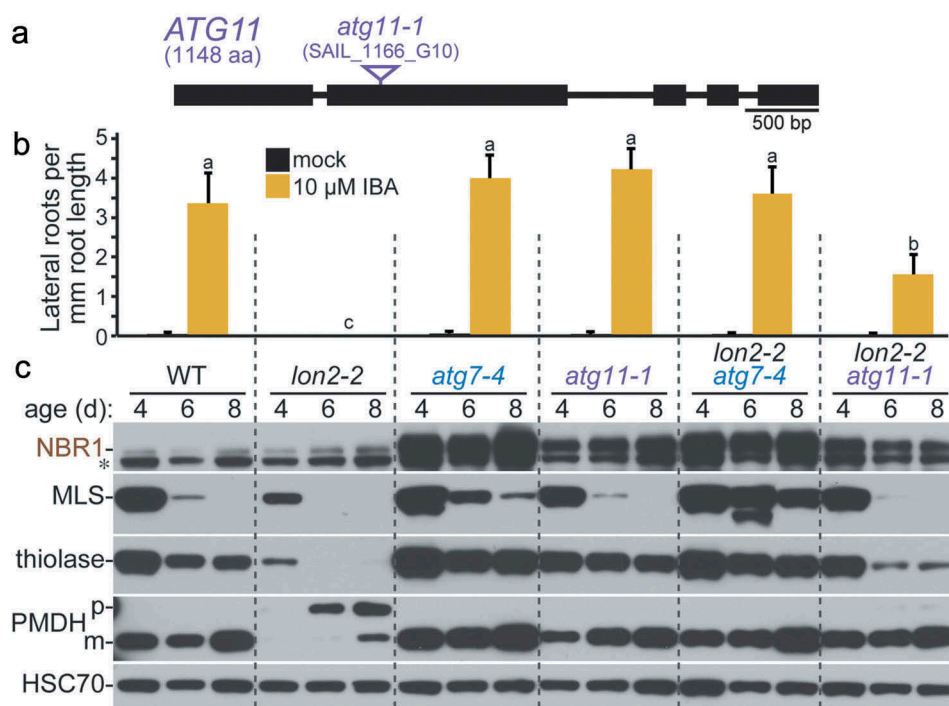


Figure 6. Loss of ATG11 partially suppresses *lon2* defects. (a) Diagram of the *ATG11* gene. Boxes and lines represent protein-coding regions and introns, respectively. A triangle marks the location of the *atg11-1* T-DNA insertion allele [17]. aa, amino acids. (b) Lateral root density of 8-day-old wild type (WT), *lon2-2*, *atg7-4*, *atg11-1*, *lon2-2 atg7-4*, and *lon2-2 atg11-1* seedlings grown without or with IBA. Error bars show standard deviations ($n = 8$). Statistically significant ($P < 0.0001$) differences determined by one-way ANOVA are depicted by different letters above the bars. (c) Extracts from 4-, 6-, and 8-day-old seedlings were processed for immunoblotting with antibodies to the indicated proteins. An asterisk indicates a protein cross-reacting with the NBR1 antibody.

ATG18a appears to act non-redundantly with the other 7 ATG18 isoforms [23] in *Arabidopsis* seedling pexophagy. The *atg18a-3* and *atg18a-4* nonsense alleles fully restored *lon2-2* IBA responsiveness and PTS2 processing, and *lon2-2 atg18a* seedlings displayed similarly stabilized NBR1, MLS, and thiolase as other *lon2-2 atg* double mutants (Figure 4(d, e)). In addition, ATG8 elevation in *atg18a-3* was similar to the elevation in *atg2-6* (Figure 3(d)). Moreover, the increased peroxisome abundance in *atg18a-3* seedlings (Figure 5) and the isolation of an *atg18a* mutant from a microscopy-based screen for aggregated peroxisomes [15] are consistent with a requirement for ATG18a in pexophagy. ATG18a functions beyond pexophagy; RNAi-based *ATG18a* downregulation confers hypersensitivity to starvation [23] and various abiotic stresses [11,12]. Although most of the ATG18 isoforms are upregulated during seed maturation [13], whether the remaining 7 *Arabidopsis* ATG18 isoforms [23] function in autophagy remains an open question.

Because no *atg11* mutants emerged from our screen for *lon2-2* suppressors, we crossed the *atg11-1* T-DNA insertional allele to *lon2-2* and observed only partial suppression of *lon2-2* phenotypes (Figure 6), suggesting that pexophagy is incompletely blocked in *atg11-1*. This conclusion is supported by the observation that *atg11-1* accumulates less catalase than other *atg* mutants [18]. Moreover, ATG8 and NBR1 are only partially stabilized in *atg11-1* relative to *atg7-4* and other null alleles in core ATG genes (Figure 3(d), 6(c)), consistent with previous reports that autophagy is incompletely blocked in *atg11-1* [17,18]. As ATG11 is thought to act as a scaffold for ATG1a and ATG13 within the phagophore assembly site [17],

these findings imply that autophagy can still occur, albeit less efficiently, in *atg11-1* seedlings. Despite the large size of ATG11 (1148 amino acids), its role as a scaffold may allow some tolerance for missense mutations, which, combined with the observation that *atg11-1* only partially restored *lon2-2* IBA responsiveness (Figure 6(b)), may explain why *atg11* mutants did not emerge from *lon2-2* suppressor screens. In *Pichia pastoris*, Atg11 binds both Atg8 and the pexophagy receptor Atg30 [78], so it will be interesting to determine whether ATG11 plays a similar role in *Arabidopsis* pexophagy. *Arabidopsis* ATG11 also interacts with ATG8 [17], and additional studies are needed to decipher the role of this protein in processes upstream and downstream of ATG8 lipidation.

Besides *ATG11*, mutants of 5 other single-copy *Arabidopsis* ATG orthologs did not emerge from our *lon2-2* suppressor screen: *ATG6/At3g61710*, *ATG9/At2g31260*, *ATG10/At3g07525*, *ATG20/At5g0614*, and *ATG101/At5g66930*. Of these 5, only the putative *ATG20* ortholog *SNX1* (Sorting Nexin 10), which acts in endosomal sorting [79], has not been directly implicated in autophagy in plants. Conversely, although *Arabidopsis* *ATG6* is important for autophagy [21], *atg6* defects in pollen germination confer male sterility [80,81] that would preclude recovery from our *lon2-2* suppressor screen. *Arabidopsis* *ATG9* is a transmembrane protein critical for autophagosome formation [24,82–84], but autophagic flux is only partially compromised in *atg9* mutants [18,82]. It would be interesting to determine whether *atg9* mutants partially suppress *lon2-2* similar to *atg11* mutants (Figure 6). *ATG10* is an E2-like enzyme

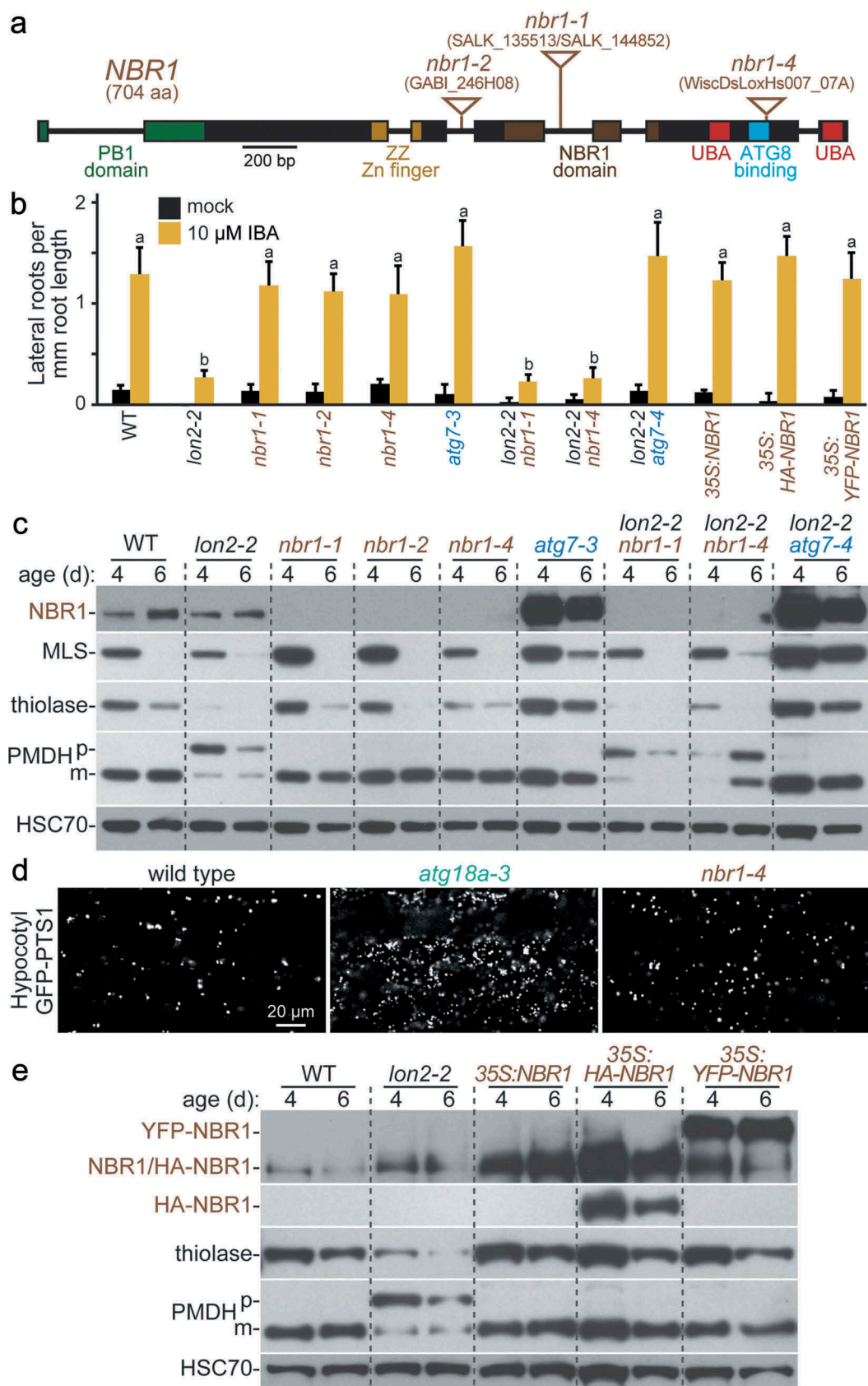


Figure 7. NBR1 is not necessary for pexophagy of *lon2* peroxisomes, and excess NBR1 is not sufficient to induce pexophagy. (a) Diagram of the *NBR1* gene. Boxes and lines represent protein-coding regions and introns, respectively. The PB1 domain, zinc finger, NBR1 domain, ATG8 binding site, and ubiquitin-associated (UBA) domains are indicated. Triangles mark the locations of T-DNA insertion alleles. aa, amino acids. (b) Lateral root density of 8-day-old wild type (WT), *lon2-2*, *nbr1*, *atg7-3*, *lon2-2 nbr1*, *lon2-2 atg7-4*, *35S:NBR1*, *35S:HA-NBR1*, and *35S:YFP-NBR1* seedlings grown without or with IBA. Error bars show standard deviations ($n = 8$). Statistically significant ($P < 0.0001$) differences determined by one-way ANOVA are depicted by different letters above the bars. (c) Extracts prepared from 4- and 6-day-old seedlings were processed for immunoblotting with antibodies to the indicated proteins. (d) Hypocotyl cells in 6-day-old wild-type, *atg18a-3*, and *nbr1-4* light-grown seedlings expressing the peroxisomal matrix marker GFP-PTS1 were imaged for GFP fluorescence using confocal microscopy. Scale bar: 20 μm . (e) Extracts prepared from 4- and 6-day-old seedlings were processed for immunoblotting with antibodies to the indicated proteins.

that conjugates ATG12 during autophagosome formation and is essential for *Arabidopsis* autophagy [30]. ATG101 interacts with ATG11 and ATG13a [17], but *atg101* mutants have not been described. The genes encoding ATG10 (226 amino acids) and ATG101 (215 amino acids) are relatively small targets for EMS mutagenesis, so further screening might yield mutants of these genes.

In addition to *ATG18*, several *ATG* genes are present as gene families in *Arabidopsis*: *ATG1* (3 genes), *ATG4* (2 genes), *ATG8* (9 genes), *ATG12* (2 genes), and *ATG13* (2 genes). The roles of these genes in *Arabidopsis* autophagy have been experimentally validated using reverse-genetic and biochemical approaches [7,8,27,84,85]. The failure of these genes to emerge from forward-genetic screens for *lon2-2* suppressors is consistent with the possibility that, unlike *ATG18a* (Figure 4), the genes in these families function redundantly in pexophagy.

Arabidopsis pexophagy receptors remain to be identified

In spite of the conservation of autophagy across kingdoms, identified pexophagy receptors differ among species, and a pexophagy receptor has not been reported in plants. *Pichia pastoris* Atg30 [86] and *Saccharomyces cerevisiae* Atg36 [87] act as pexophagy receptors, but plants lack Atg30 or Atg36 orthologs. We did not recover mutants of candidate pexophagy receptors in our screen for *lon2-2* suppressors. Because NBR1 is a pexophagy receptor in mammalian cells [67] and a selective autophagy receptor in *Arabidopsis* [10,14,36,37], we used reverse genetics to investigate the role of *Arabidopsis* NBR1 in pexophagy. Two T-DNA insertional alleles of *nbr1* failed to suppress *lon2-2* defects (Figure 7(b, c)), and NBR1 overexpression failed to phenocopy *lon2* seedling defects (Figure 7(b, e)), which presumably result from heightened pexophagy. Moreover, peroxisome abundance in *nbr1-4* seedlings resembled wild type rather than the increased abundance of peroxisomes observed in *atg18a-3* (Figure 7(d)). These data indicate that NBR1 is not the sole pexophagy receptor in *lon2* seedlings but do not eliminate the possibility that NBR1 acts redundantly in pexophagy or in other contexts. Intriguingly, peroxisomal catalase accumulates in *nbr1* mutants during heat stress [36], suggesting that NBR1 might be important for LON2-independent pexophagy in *Arabidopsis*. Further studies are needed to fully elucidate the roles of NBR1 in *Arabidopsis* selective autophagy.

Perhaps plants employ a pexophagy receptor that is distinct from those identified in yeast and mammalian cells. The plant-specific ATI (ATG8-interacting) proteins [39,40] are pexophagy receptor candidates but did not emerge from our screen for *lon2-2* suppressors. The ubiquitin-binding protein DSK2 [88] is another pexophagy receptor candidate in *Arabidopsis*. *Arabidopsis* DSK2 binds to and targets the transcription factor BES1 for autophagic degradation [42]. DSK2 also interacts with 2 peroxisomal membrane proteins [89]. Because *Arabidopsis* has 2 *DSK2* paralogs (*At2g17190* and *At2g17200*) [90], recovering *dsk2* mutants as *lon2* suppressors is unlikely, and directed approaches will be needed to explore the potential roles of DSK2 and ATI proteins in pexophagy.

Potential roles for peroxins in pexophagy

PEX (peroxin) proteins are necessary for peroxisome biogenesis and matrix protein import [91]; many peroxins are found on the peroxisome membrane where they would be accessible to the autophagy machinery. Several peroxins have been implicated in pexophagy in *Arabidopsis* as well as yeast and mammalian cells. In general, peroxins or other peroxisomal membrane proteins might mediate pexophagy in 3 ways.

First, post-translationally modified peroxins could interact with a selective autophagy receptor. In mammalian cells, PEX5 phosphorylation by ataxia-telangiectasia mutated (ATM) leads to pexophagy [92]. Selective autophagy receptors, including NBR1, often recognize ubiquitinated cargo [4,33]. Because the matrix protein import peroxin PEX5 is ubiquitinated during its typical function [93], ubiquitinated PEX5 is a candidate pexophagy signal.

Second, peroxisomal membrane proteins could interact directly with a selective autophagy receptor. For example, *Pichia pastoris* Atg37 is a peroxisomal membrane protein that binds to the pexophagy receptor Atg30 and modulates pexophagy [94,95]. Moreover, the membrane peroxins Pex3 and Pex14 interact with the *P. pastoris* pexophagy receptor Atg30 [86,94,96]. Pex3 also binds to the *Saccharomyces cerevisiae* pexophagy receptor Atg36 [87], and PEX3 plays a pivotal role in pexophagy in mammalian cells [97]. Decreasing PEX14 levels in mammalian cells reduces pexophagy, perhaps as a result of reduced recruitment of PEX5 [67]. In *Arabidopsis*, the membrane peroxins PEX2/At1g79810 and PEX12/At3g04460 interact with DSK2 [89], making these peroxins candidates for pexophagy regulators.

Third, peroxins could interact directly with ATG8, bypassing the need for a bridging receptor. Although the relative simplicity of ATG8-interacting motifs has confounded bioinformatic approaches to identifying ATG8-interacting proteins, a recent refinement considering acidic residue positioning reveals that *Arabidopsis* PEX10/At2g26350 and PEX6/At1g03000 interact with ATG8 [34]. Interestingly, pexophagy contributes to defects observed in *pex1* and *pex6* mutants in *Arabidopsis* [98,99], yeast [100], and humans [101], suggesting that PEX6 prevents rather than promotes pexophagy, perhaps by competing with the pexophagy signal for interaction with ATG8 or by removing ubiquitinated substrates, such as PEX5, from the peroxisomal surface.

Despite the potential importance of peroxins in pexophagy, *pex* mutants are unlikely to emerge as *lon2-2* suppressors because *pex* mutants are generally IBA resistant [91] and thus not expected to restore IBA-responsive lateral rooting to *lon2* (Figure 1(a)). Alternative approaches will be needed to dissect the roles of peroxins in *Arabidopsis* pexophagy.

Conclusions

We used forward genetics to recover 21 alleles of 6 *ATG* genes. All 6 genes are core *ATG* genes, underscoring the functional conservation of these components. These mutant alleles will be useful in future studies interrogating the role of these genes in *Arabidopsis* autophagy, especially the *atg3*

and *atg16* alleles, which disrupt genes without available T-DNA insertional alleles. Using the *lon2* mutant as a system for studying pexophagy in *Arabidopsis*, we also investigated the role of ATG11 and NBR1 in this process and found that ATG11 plays a limited role in pexophagy whereas NBR1 does not appear to be involved in *lon2*-related pexophagy. *lon2* mutants will undoubtedly serve as a useful platform for future studies elucidating the regulation of pexophagy in *Arabidopsis*.

Materials and methods

Plant material and growth conditions

The Columbia-0 (Col-0) accession of *Arabidopsis thaliana* transformed with 35S:*GFP-PTS1* [66] was used as the wild-type control. *lon2-2* (SALK_043857) [49] crossed to 35S:*GFP-PTS1* was mutagenized to isolate suppressors (see Mutant Isolation below) and used as the *lon2-2* control for subsequent experiments. *lon2-2 atg2-4 35S:PTS2-GFP* and *lon2-2 atg7-4 35S:PTS2-GFP* were previously described [48]. *atg7-3* (SAIL_11_H07) [9,22], *atg11-1* (SAIL_1166_G10) [17], *nbr1-1* (SALK_135513) [10], and *nbr1-2* (GABI_246H08) [10] were previously described and were obtained from the *Arabidopsis* Biological Resource Center (ABRC) at Ohio State University. We found that the T-DNA interrupting *NBR1* in SALK_144852 (Figure 7(a)) was at the identical position as the T-DNA in *nbr1-1* (SALK_135513). *lon2-2 atg7-9 35S:PTS2-GFP* is an unpublished allele originating from a screen for *lon2-2 35S:PTS2-GFP* suppressors [48]. *atg2-4 35S:PTS2-GFP*, *atg3-1 35S:PTS2-GFP*, and *atg7-4 35S:PTS2-GFP* were obtained by crossing the respective *lon2-2 atg 35S:PTS2-GFP* double mutant [48] to 35S:*PTS2-GFP* [102] to remove the *lon2-2* mutation. *atg2-6 35S:GFP-PTS1*, *atg5-5 35S:GFP-PTS1*, *atg16-3 35S:GFP-PTS1*, and *atg18a-3 35S:GFP-PTS1* were obtained by crossing the respective *lon2-2 atg 35S:GFP-PTS1* double mutant to 35S:*GFP-PTS1* to remove the *lon2-2* mutation. The presence of the T-DNA insertion in *atg11-1*, *lon2-2*, *nbr1-1*, and *nbr1-2* was confirmed by PCR of genomic DNA using a gene-specific primer and a T-DNA left-border specific primer (Table S1).

nbr1-4 (WiscDsLoxHs007_07A) was obtained from the ABRC. The position of the T-DNA insertion was confirmed by PCR of genomic DNA using a gene-specific primer and a T-DNA left-border specific primer (Table S1), and the exact position of the insertion was determined by sequencing the PCR product (Lone Star Labs, Houston, TX, USA). *nbr1-4 35S:GFP-PTS1* was obtained by crossing.

To generate NBR1-overexpressing lines, an *NBR1* cDNA in pENTR223 (stock G25119) from the ABRC was cloned using LR Clonase II (Invitrogen, 11791020) into pEarleyGate destination vectors pEG100, pEG104, and pEG201 [103] from the ABRC. The resultant 35S:*NBR1*, 35S:*YFP-NBR1*, and 35S:*HA-NBR1* plasmids were used to transform *Agrobacterium tumefaciens* GV3101 (pMP90) [104] by electroporation. The resultant *A. tumefaciens* strains were used to transform Col-0 plants using the floral dip method [105]. Transformed plants were selected for glufosinate ammonium (Basta, Gold Biotechnology, P-165-1) resistance, and overexpression was

confirmed by immunoblot analysis using anti-NBR1 [14]. Homozygous progeny were used for phenotypic analysis.

Seeds were surface-sterilized using 3% (w:v) sodium hypochlorite solution containing 0.01% (v:v) Triton X-100 (Sigma-Aldrich, T9284), resuspended in 0.1% agar (Fisher Scientific, BD-214030), and stratified at 4°C overnight. Seedlings were grown at 22°C on plant nutrient (PN) medium [106] supplemented with 0.5% (w:v) sucrose (VWR, JT4097-6) (PNS) and solidified with 0.6% (w:v) agar. To quantify IBA sensitivity, seedlings were grown on PNS plates under continuous white light for 4 days, transferred to new PNS plates with either ethanol (mock) or 10 μM IBA (Sigma-Aldrich, I5386; made from a 100-mM stock in ethanol), and grown under light filtered with yellow long-pass filters (to slow photochemical breakdown of indolic compounds) [107] for an additional 4 days. Lateral roots emerged from the primary root were counted using a stereomicroscope (S6E, Leica Microsystems, Buffalo Grove, IL, USA), and primary root lengths were measured using a ruler. Measurements were completed at least twice with similar results.

Mutant isolation

lon2-2 35S:GFP-PTS1 seeds (1.3 g, ~65,000 seeds) were mutagenized for 16 h at room temperature with 0.24% to 0.25% (v:v) ethylmethane sulfonate (Sigma-Aldrich, M0880), rinsed extensively with water, and grown in 104 M₁ pools. For screening, 0.1 g of M₂ seeds (~5000 seeds) per pool were surface-sterilized, stratified, and plated on PNS medium supplemented with 8 μM IBA and solidified with 1.0% (w:v) agar in square Petri dishes (89 x 89 mm). Plates were positioned vertically, and seedlings were grown under yellow-filtered light for 8 days, when M₂ seedlings with 3 or more lateral roots were moved to soil. Leaf tissue was collected from approximately 30-day-old M₂ plants for immunoblot analysis using anti-PMDH, anti-NBR1, anti-ATG7, and anti-HSC70 antibodies (as described below). M₃ seeds from M₂ plants with multiple lateral roots, complete PTS2 processing, and elevated NBR1 protein levels were collected and re-tested for IBA resistance (as described above in Plant Materials and Growth Conditions), and 6-day-old tissue was tested by immunoblot analysis using anti-thiolase, anti-ATG3, anti-HSC70, and anti-ICL or anti-MLS (as described below). Lines exhibiting IBA sensitivity and thiolase and ICL or MLS stabilization were retained as *lon2* suppressors. All suppressors were genotyped to confirm *lon2-2* homozygosity (Table S1). After suppressor mutation identification, PCR-based genotyping markers designed using dCAPS Finder 2.0 [108] were used to confirm the presence of the identified lesions (Table S2) and follow mutations in the progeny of crosses.

Whole-genome sequencing

Genomic DNA from 10 suppressors was prepared for whole-genome sequencing. Genomic DNA from 6 suppressors (*atg2-6*, *atg5-6*, *atg7-19*, *atg16-1*, *atg16-2*, and *atg16-3*) was prepared from F₂ seedlings from lines backcrossed to *lon2-2 35S:GFP-PTS1*. Surface-sterilized F₂ seeds were plated on PNS medium supplemented with 8 μM IBA and solidified with 0.6% (w:v) agar and grown at 22°C under light filtered with yellow long-

pass filers. At 10 days, between 50 and 100 F₂ seedlings with lateral roots were moved to sterile filter paper atop PNS medium and grown at 22°C under white light for approximately 15 more days before collecting tissue. Genomic DNA from one suppressor (*atg5-5*) was prepared from F₃ seedlings pooled from 3 F₃ lines from a backcross to *lon2-2 35S:GFP-PTS1*, and genomic DNA from 3 suppressors (*atg2-7*, *atg18a-3*, and *atg18a-4*) was prepared from un-backcrossed lines.

Genomic DNA for whole-genome sequencing was prepared as previously described [109]. DNA was sequenced with HiSeq2500 sequencers (Illumina, San Diego, CA, USA) at the Genome Technology Access Center at Washington University in St. Louis and aligned with the TAIR 10 build of the *A. thaliana* Col-0 genome using Novoalign (Novocraft; <http://novocraft.com>). SNPs were identified using SAMtools [110] and annotated with snpEFF [111]. Mutations were filtered using a script that prioritized homozygous canonical EMS-derived mutations (G-to-A and C-to-T) causing non-synonymous amino acid changes or altered splice sites but also retained mutations in introns and heterozygous EMS-consistent mutations. We disregarded mutations that were present in our lab stock of Col-0 or in multiple suppressors from different pools, indicating an origin in the starting line. Chromosomal nucleotide positions and gene identifiers of genes with homozygous EMS-consistent mutations are listed in Data S1.

Sequencing genomic DNA from the L1 isolate revealed mutations in both *ATG18a* (c463t causing Q155Stop) and *ATG18f* (g708a causing A198T). To determine which of these lesions was linked to *lon2* suppression, we crossed L1 to *lon2-2 35S:GFP-PTS1* and used genotyping markers (Table S2) to isolate F₃ plants that were homozygous for the *atg18a* lesion but homozygous for wild-type *ATG18f* and vice versa. The resultant F₄ progeny were tested for IBA responsive lateral rooting and 6-day-old immunoblot phenotypes to reveal that the *atg18a* mutation suppressed *lon2-2* whereas the *atg18f* mutation did not alter *lon2-2* phenotypes. We used the backcrossed *lon2-2 atg18a-3* mutant in subsequent analyses.

Individual gene sequencing

ATG7 or *ATG3* was sequenced directly in suppressors with reduced *ATG7* or *ATG3* protein levels, respectively. *ATG7* was PCR amplified using the primers indicated in Table S3, and *ATG3* was PCR amplified using previously described primers [48]. Amplicons were purified using the DNA Clean & Concentrator kit (Zymo Research, D4004) and sequenced directly (Lone Star Labs, Houston, TX, USA or Genewiz, Houston, TX, USA) with the primers used for amplification.

Immunoblot analysis

For most immunoblots, extracts were prepared from seedlings or adult leaves by homogenizing frozen tissue in 2 volumes of 2X NuPAGE LDS sample buffer (212 mM Tris HCl [Fisher Scientific, BP1531], 282 mM Tris base [Fisher Scientific, BP1525], 4% [w:v] lithium dodecyl sulfate [Worldwide Medical Products, 0782], 1.02 mM EDTA [Genesee Scientific, 20-148], 20% [w:v] glycerol [Worldwide Medical Products, 0854],

0.44 mM Coomassie Brilliant Blue G250 [Bio-Rad 161-0406], 0.332 mM Phenol Red [Sigma-Aldrich P5530], pH 8.5) containing 50 mM dithiothreitol (Gold Biotechnology, DTT10) and heating at 100°C for 5 min. Samples were electrophoresed on Bolt 10% Bis-Tris Plus gels (Invitrogen, NW00100BOX/NW00102BOX/NW00107BOX) or NuPAGE 10% Bis-Tris Midi gels (Invitrogen, WG1202BOX) using 1X MOPS running buffer (50 mM MOPS [Gold Biotechnology, M-790-1], 50 mM Tris base, 0.1% SDS [Dot Scientific, DSL22010], 1 mM EDTA, pH 7.7) and transferred to Amersham Protran Premium nitrocellulose membrane (VWR, 10120-006) for 40 min at 24 V using NuPAGE transfer buffer (25 mM Bicine [Gold Biotechnology, B-785-1], 25 mM Bis-Tris [Gold Biotechnology, B-020-1], 1 mM EDTA, 0.05 mM Chlorobutanol [Sigma-Aldrich 11,205-4], 10% [v:v] methanol, pH 7.2).

For ATG8 immunoblot analysis (Figure 3(d)), extracts were prepared by homogenizing frozen seedlings in 2 volumes of 2X Tricine SDS sample buffer (900 mM Tris HCl, 24% glycerol, 8% SDS, 0.005% Coomassie Brilliant Blue G250, 0.005% Phenol Red, pH 8.45) containing 6 M urea (JT Baker, 4204-01) and 50 mM dithiothreitol. Samples were electrophoresed on 10% Tricine gels (Invitrogen, EC66752BOX) using 1X Tricine SDS running buffer (100 mM Tris base, 100 mM Tricine [Sigma-Aldrich T0377], 0.1% SDS, pH 8.3) and transferred to Amersham Protran Premium nitrocellulose membrane for 1 h at 24 V using Tris-glycine transfer buffer (12 mM Tris base, 96 mM glycine, 20% [v:v] methanol, pH 8.3).

Membranes were blocked in 8% (w:v) Carnation non-fat dry milk solution (or 5% [w:v] bovine serum albumin [Gibco-BRL, 11018-017] for the anti-ATG3 and anti-ATG5 antibodies) in 20 mM Tris, pH 7.5, 150 mM NaCl, 0.1% Tween 20 (Promega, H5151) and then incubated overnight at 4°C with primary antibodies in blocking solution. Rabbit antibodies against ATG3 [30] (1:10,000), ATG5 (1:2000; Agrisera, AS15 3060), ATG7 [8] (1:1000), ATG8A (1:2500; Abcam, ab77003; previously known as APG8A), ICL [112] (1:1000), MLS [113] (1:25,000), NBR1 [14] (1:2000), the PED1 isoform of thiolase [114] (1:20,000), and PMDH2 [115] (1:5000) were diluted as indicated. Mouse antibodies against HSC70 (1:100,000; StressGen Bioreagents, SPA-817) were used. Primary antibodies were visualized with goat anti-rabbit (1:5000; Santa Cruz Biotechnology, SC-2030 or GenScript, A00098) or anti-mouse (1:5000; Santa Cruz Biotechnology, SC-516102) horseradish peroxidase-conjugated secondary antibodies diluted in blocking buffer. Horseradish peroxidase was visualized with ProSignal Pico ECL reagent (Genesee Scientific, 20-300B) and autoradiography film (Genesee Scientific, 30-810C). Membranes were reblocked and sequentially probed with the indicated antibodies without stripping the membrane between incubations.

Confocal fluorescence microscopy

Wild-type *35S:GFP-PTS1*, *atg18a-3 35S:GFP-PTS1*, and *nbr1-4 35S:GFP-PTS1* seedlings grown on PNS under continuous white light were mounted in water, and fluorescence was visualized using a LSM 710 laser scanning confocal microscope (Carl Zeiss Microscopy, Thornwood, NY, USA) equipped with a meta detector. Samples were imaged using a 63X (Figure 5) or 40X

(Figure 7(d)) oil immersion objective. GFP and chlorophyll were excited with a 488-nm argon laser. GFP emission was collected between 493 nm and 572 nm, and chlorophyll autofluorescence was collected between 620 nm and 719 nm. Each image in Figure 5 is an average of 2 exposures using a 47- μ m pinhole, corresponding to a 0.8- μ m optical section. Each image in Figure 7(d) is an average of 4 exposures using a 47- μ m pinhole, corresponding to a 1.2- μ m optical section.

Statistical analysis

One-way ANOVA with the Duncan post-hoc test was used to assess statistical significance (SPSS Statistics software, Version 24.0.0.0).

Accession numbers

Sequence data can be found in the *Arabidopsis* Genome Initiative under the following accession numbers: *At3g19190* (*ATG2*), *At5g61500* (*ATG3*), *At5g17290* (*ATG5*), *At5g45900* (*ATG7*), *At4g30790* (*ATG11*), *At5g50230* (*ATG16*), *At3g62770* (*ATG18a*), *At5g47040* (*LON2*), and *At4g24690* (*NBR1*). The Brassicaceae *ATG2* orthologs used for alignment have the following accession numbers: EFH59425.1 (*Arabidopsis lyrata*), XP_013585639.1 (*Brassica oleracea*), XP_009145821.1 (*Brassica rapa*), XP_006296813.1 (*Capsella rubella*), and XP_006406527.1 (*Eutrem salsugineum*).

Acknowledgments

We thank Hiba Zafar for assistance with screening and Charles Danan for assistance with identifying *lon2-2 atg7-9 35S:PTS2-GFP*. We thank Yun-Ting Kao and Joseph Faust for the script for facilitating analysis of whole-genome sequencing data and Lucia Strader (Washington University in St. Louis) for assistance with whole-genome sequencing. We thank Richard Vierstra (Washington University in St. Louis) for the anti-*ATG3* and anti-*ATG7* antibodies, Masayoshi Maeshima (Nagoya University) for the anti-*ICL* antibody, John Harada (University of California, Davis) for the anti-*MLS* antibody, Terje Johansen (University of Tromsø) for the anti-*NBR1* antibody, and Steven Smith (University of Western Australia) for the anti-*PMDH2* antibody. We thank Janet Braam, Kathryn Smith, Melissa Traver, Andrew Woodward, and Zachary Wright for critical comments on the manuscript.

Disclosure statement

No potential conflict of interest was reported by the authors.

Funding

This research was supported by the National Science Foundation (MCB-1516966) and the Robert A. Welch Foundation (C-1309). RJL was supported in part by the National Institutes of Health (F31GM125367). Genomic sequencing at the Genome Technology Access Center at Washington University School of Medicine was supported by the National Institutes of Health (P30CA91842 and UL1RR024992). Confocal microscopy equipment was obtained through a Shared Instrumentation Grant from the National Institutes of Health (S10RR026399).

ORCID

Pierce G. Young <http://orcid.org/0000-0002-1506-4053>
Bonnie Bartel <http://orcid.org/0000-0002-6367-346X>

References

- [1] Reggiori F, Klionsky DJ. Autophagic processes in yeast: mechanism, machinery and regulation. *Genetics*. 2013 Jun;194(2):341–361. PMID: 23733851; PMCPMC3664846
- [2] Mizushima N, Levine B. Autophagy in mammalian development and differentiation. *Nat Cell Biol*. 2010 Sep;12(9):823–830. PMID: 20811354; PMCPMC3127249
- [3] Li F, Vierstra RD. Autophagy: A multifaceted intracellular system for bulk and selective recycling. *Trends Plant Sci*. 2012 Sep;17(9):526–537. PMID: 22694835
- [4] Michaeli S, Galili G, Genschik P, et al. Autophagy in plants—what’s new on the menu? *Trends Plant Sci*. 2016;21(2):134–144.
- [5] Meijer WH, van der Klei IJ, Veenhuis M, et al. ATG genes involved in non-selective autophagy are conserved from yeast to man, but the selective Cvt and pexophagy pathways also require organism-specific genes. *Autophagy*. 2007 Mar-Apr;3(2):106–116. PMID: 17204848
- [6] Yoshimoto K. Beginning to understand autophagy, an intracellular self-degradation system in plants. *Plant Cell Physiol*. 2012 Aug;53(8):1355–1365. PMID: 22764279
- [7] Suttangkakul A, Li F, Chung T, et al. The ATG1/ATG13 protein kinase complex is both a regulator and a target of autophagic recycling in *Arabidopsis*. *Plant Cell*. 2011 Oct;23(10):3761–3779. PMID: 21984698; PMCPMC3229148.
- [8] Doelling JH, Walker JM, Friedman EM, et al. The APG8/12-activating enzyme APG7 is required for proper nutrient recycling and senescence in *Arabidopsis thaliana*. *J Biol Chem*. 2002 Sep 6;277(36):33105–33114. PMID: 12070171.
- [9] Lai Z, Wang F, Zheng Z, et al. A critical role of autophagy in plant resistance to necrotrophic fungal pathogens. *Plant J*. 2011 Jun;66(6):953–968. PMID: 21395886.
- [10] Zhou J, Wang J, Cheng Y, et al. NBR1-mediated selective autophagy targets insoluble ubiquitinated protein aggregates in plant stress responses. *PLoS Genet*. 2013;9(1):e1003196. PMID: 23341779; PMCPMC3547818.
- [11] Liu Y, Xiong Y, Bassham DC. Autophagy is required for tolerance of drought and salt stress in plants. *Autophagy*. 2009 Oct;5(7):954–963. PMID: 19587533
- [12] Xiong Y, Contento AL, Nguyen PQ, et al. Degradation of oxidized proteins by autophagy during oxidative stress in *Arabidopsis*. *Plant Physiol*. 2007 Jan;143(1):291–299. PMID: 17098847; PMCPMC1761971.
- [13] Di Berardino J, Marmagne A, Berger A, et al. Autophagy controls resource allocations and protein storage accumulation in *Arabidopsis* seeds. *J Exp Bot*. 2018;69(6):1403–1414.
- [14] Svenning S, Lamark T, Krause K, et al. Plant NBR1 is a selective autophagy substrate and a functional hybrid of the mammalian autophagic adapters NBR1 and p62/SQSTM1. *Autophagy*. 2011 Sep;7(9):993–1010. PMID: WOS:000294477100007.
- [15] Shibata M, Oikawa K, Yoshimoto K, et al. Highly oxidized peroxisomes are selectively degraded via autophagy in *Arabidopsis*. *Plant Cell*. 2013 Dec;25(12):4967–4983. PMID: 24368788; PMCPMC3903999.
- [16] Kim J, Lee H, Lee HN, et al. Autophagy-related proteins are required for degradation of peroxisomes in *Arabidopsis* hypocotyls during seedling growth. *Plant Cell*. 2013 Dec;25(12):4956–4966. PMID: 24368791; PMCPMC3903998.
- [17] Li F, Chung T, Vierstra RD. AUTOPHAGY-RELATED11 plays a critical role in general autophagy- and senescence-induced mitophagy in *Arabidopsis*. *Plant Cell*. 2014 Feb;26(2):788–807. PMID: 24563201; PMCPMC3967041
- [18] Kang S, Shin KD, Kim JH, et al. Autophagy-related (ATG) 11, ATG9 and the phosphatidylinositol 3-kinase control ATG2-mediated formation of autophagosomes in *Arabidopsis*. *Plant Cell Rep*. 2018 Apr;37(4):653–664. PMID: 29350244.

- [19] Suzuki K, Kubota Y, Sekito T, et al. Hierarchy of Atg proteins in pre-autophagosomal structure organization. *Genes Cells*. 2007 Feb;12(2):209–218. PMID: 17295840.
- [20] Kihara A, Noda T, Ishihara N, et al. Two distinct Vps34 phosphatidylinositol 3-kinase complexes function in autophagy and carboxypeptidase Y sorting in *Saccharomyces cerevisiae*. *J Cell Biol*. 2001 Feb 5;152(3):519–530. PMID: 11157979; PMCPMC2196002
- [21] Patel S, Dinesh-Kumar SP. *Arabidopsis* ATG6 is required to limit the pathogen-associated cell death response. *Autophagy*. 2008 Jan 1;4(1):20–27. PMID: WOS:000252211800003.
- [22] Wang Y, Nishimura MT, Zhao T, et al. ATG2, an autophagy-related protein, negatively affects powdery mildew resistance and mildew-induced cell death in *Arabidopsis*. *Plant J*. 2011 Oct;68(1):74–87. PMID: 21645148.
- [23] Xiong Y, Contento AL, Bassham DC. AtATG18a is required for the formation of autophagosomes during nutrient stress and senescence in *Arabidopsis thaliana*. *Plant J*. 2005 May;42(4):535–546. PMID: WOS:000228746000008
- [24] Zhuang X, Chung KP, Cui Y, et al. ATG9 regulates autophagosome progression from the endoplasmic reticulum in *Arabidopsis*. *Proc Natl Acad Sci USA*. 2017 Jan 17;114(3):E426–E425. PMID: 28053229; PMCPMC5255614.
- [25] Sláviková S, Shy G, Yao Y, et al. The autophagy-associated Atg8 gene family operates both under favourable growth conditions and under starvation stresses in *Arabidopsis* plants. *J Exp Bot*. 2005;56(421):2839–2849.
- [26] Ohsumi Y. Molecular dissection of autophagy: two ubiquitin-like systems. *Nat Rev Mol Cell Biol*. 2001 Mar;2(3):211–216. PMID: 11265251.
- [27] Chung T, Phillips AR, Vierstra RD. ATG8 lipidation and ATG8-mediated autophagy in *Arabidopsis* require ATG12 expressed from the differentially controlled *ATG12A* and *ATG12B* loci. *Plant J*. 2010 May;62(3):483–493. PMID: 20136727
- [28] Yoshimoto K, Hanaoka H, Sato S, et al. Processing of ATG8s, ubiquitin-like proteins, and their deconjugation by ATG4s are essential for plant autophagy. *Plant Cell*. 2004 Nov;16(11):2967–2983. PMID: WOS:000225228500010.
- [29] Thompson AR, Doelling JH, Suttangkakul A, et al. Autophagic nutrient recycling in *Arabidopsis* directed by the ATG8 and ATG12 conjugation pathways. *Plant Physiol*. 2005 Aug;138(4):2097–2110. PMID: 16040659; PMCPMC1183398.
- [30] Phillips AR, Suttangkakul A, Vierstra RD. The ATG12-conjugating enzyme ATG10 is essential for autophagic vesicle formation in *Arabidopsis thaliana*. *Genetics*. 2008 Mar;178(3):1339–1353. PMID: WOS:000254921600022
- [31] Romanov J, Walczak M, Ibric I, et al. Mechanism and functions of membrane binding by the Atg5-atg12/Atg16 complex during autophagosome formation. *Embo J*. 2012;31(22):4304–4317.
- [32] Yamaguchi M, Matoba K, Sawada R, et al. Noncanonical recognition and UBL loading of distinct E2s by autophagy-essential Atg7. *Nat Struct Mol Biol*. 2012 Dec;19(12):1250–1256. PMID: 23142983.
- [33] Rogov V, Dotsch V, Johansen T, et al. Interactions between autophagy receptors and ubiquitin-like proteins form the molecular basis for selective autophagy. *Mol Cell*. 2014 Jan 23;53(2):167–178. PMID: 24462201.
- [34] Xie Q, Tzfadia O, Levy M, et al. hFAIM: A reliable bioinformatics approach for in silico genome-wide identification of autophagy-associated ATG8-interacting motifs in various organisms. *Autophagy*. 2016;12(5):876–887. PMID: WOS:000375330100010.
- [35] Zientara-Rytter K, Lukomska J, Moniuszko G, et al. Identification and functional analysis of Joka2, a tobacco member of the family of selective autophagy cargo receptors. *Autophagy*. 2011 Oct;7(10):1145–1158. PMID: 21670587; PMC3242614.
- [36] Zhou J, Zhang Y, Qi J, et al. E3 ubiquitin ligase CHIP and NBR1-mediated selective autophagy protect additively against proteotoxicity in plant stress responses. *PLoS Genet*. 2014 Jan;10(1):e1004116. PMID: 24497840; PMC3907298.
- [37] Hafrén A, Macia J-L, Love AJ, et al. Selective autophagy limits cauliflower mosaic virus infection by NBR1-mediated targeting of viral capsid protein and particles. *Proc Natl Acad Sci USA*. 2017 Mar 7;114(10):E2026–E2035. PMID: 28223514; PMCPMC5347569.
- [38] Marshall RS, Li F, Gemperline DC, et al. Autophagic degradation of the 26S proteasome is mediated by the dual ATG8/ubiquitin receptor RPN10 in *Arabidopsis*. *Mol Cell*. 2015 Jun 18;58(6):1053–1066. PMID: WOS:000360986700017.
- [39] Honig A, Avin-Wittenberg T, Ufaz S, et al. A new type of compartment, defined by plant-specific Atg8-interacting proteins, is induced upon exposure of *Arabidopsis* plants to carbon starvation. *Plant Cell*. 2012 Jan;24(1):288–303. PMID: WOS:000300881800025.
- [40] Zhou J, Wang Z, Wang X, et al. Dicot-specific ATG8-interacting ATI3 proteins interact with conserved UBAC2 proteins and play critical roles in plant stress responses. *Autophagy*. 2018;14(3):487–504. PMID: 29313416; PMCPMC5915045.
- [41] Michaeli S, Honig A, Levanony H, et al. *Arabidopsis* ATG8-INTERACTING PROTEIN1 is involved in autophagy-dependent vesicular trafficking of plastid proteins to the vacuole. *Plant Cell*. 2014 Oct;26(10):4084–4101. PMID: WOS:000345920900023.
- [42] Nolan TM, Brennan B, Yang M, et al. Selective autophagy of BES1 mediated by DSK2 balances plant growth and survival. *Dev Cell*. 2017 Apr 10;41(1):33–46. PMID: 28399398; PMCPMC5720862.
- [43] van Den Bosch H, Schutgens RB, Wanders RJ, et al. Biochemistry of peroxisomes. *Annu Rev Biochem*. 1992;61:157–197. PMID: 1353950.
- [44] Willekens H, Chamnongpol S, Davey M, et al. Catalase is a sink for H₂O₂ and is indispensable for stress defence in C₃ plants. *Embo J*. 1997 Aug 15;16(16):4806–4816. PMID: 9305623; PMC1170116.
- [45] Anand P, Kwak Y, Simha R, et al. Hydrogen peroxide induced oxidation of peroxisomal malate synthase and catalase. *Arch Biochem Biophys*. 2009 Nov;491(1–2):25–31. PMID: 19800310.
- [46] Young PG, Bartel B. Pexophagy and peroxisomal protein turnover in plants. *BBA - Mol Cell Res*. 2016 May;1863(5):999–1005. PMID: 26348128; PMCPMC4779433
- [47] Yoshimoto K, Shibata M, Kondo M, et al. Organ-specific quality control of plant peroxisomes is mediated by autophagy. *J Cell Sci*. 2014 Mar 15;127(Pt 6):1161–1168. PMID: 24463818.
- [48] Farmer LM, Rinaldi MA, Young PG, et al. Disrupting autophagy restores peroxisome function to an *Arabidopsis lon2* mutant and reveals a role for the LON2 protease in peroxisomal matrix protein degradation. *Plant Cell*. 2013 Oct;25(10):4085–4100. PMID: 24179123; PMC3877801.
- [49] Lingard MJ, Bartel B. *Arabidopsis* LON2 is necessary for peroxisomal function and sustained matrix protein import. *Plant Physiol*. 2009 Nov;151(3):1354–1365. PMID: WOS:000271430500036
- [50] Goto-Yamada S, Mano S, Nakamori C, et al. Chaperone and protease functions of LON protease 2 modulate the peroxisomal transition and degradation with autophagy. *Plant Cell Physiol*. 2014 Mar;55(3):482–496. PMID: 24492254.
- [51] Gur E, Sauer RT. Recognition of misfolded proteins by Lon, a AAA+ protease. *Genes Dev*. 2008 Aug 15;22(16):2267–2277. PMID: 18708584; PMCPMC2518814.
- [52] Wohlever ML, Baker TA, Sauer RT. Roles of the N domain of the AAA+ Lon protease in substrate recognition, allosteric regulation and chaperone activity. *Mol Microbiol*. 2014 Jan;91(1):66–78. PMID: 24205897; PMC3877180
- [53] Aksam EB, Koek A, Jourdan S, et al. A peroxisomal Lon protease and peroxisome degradation by autophagy play key roles in vitality of *Hansenula polymorpha* cells. *Autophagy*. 2007 Mar-Apr;3(2):96–105. PMID: 17172804
- [54] Bartoszewska M, Williams C, Kikhney A, et al. Peroxisomal proteostasis involves a Lon family protein that functions as protease and chaperone. *J Biol Chem*. 2012 Aug 10;287(33):27380–27395. PMID: 22733816; PMC3431691.

- [55] Rinaldi MA, Patel AB, Park J, et al. The roles of β -oxidation and cofactor homeostasis in peroxisome distribution and function in *Arabidopsis thaliana*. *Genetics*. 2016 Nov;204(3):1089–1115. PMID: 27605050; PMCPCMC5105844.
- [56] Bartel B, Farmer LM, Rinaldi MA, et al. Mutation of the *Arabidopsis* LON2 peroxisomal protease enhances pexophagy. *Autophagy*. 2014 Mar;10(3):518–519. PMID: 24413187; PMCPCMC4077889.
- [57] Strader LC, Bartel B. Transport and metabolism of the endogenous auxin precursor indole-3-butyric acid. *Mol Plant*. 2011 February 28;2011(4):477–486.
- [58] Zolman BK, Yoder A, Bartel B. Genetic analysis of indole-3-butyric acid responses in *Arabidopsis thaliana* reveals four mutant classes. *Genetics*. 2000 Nov;156(3):1323–1337. PMID: 11063705; PMCPCMC1461311
- [59] Strader LC, Culler AH, Cohen JD, et al. Conversion of endogenous indole-3-butyric acid to indole-3-acetic acid drives cell expansion in *Arabidopsis* seedlings. *Plant Physiol*. 2010 Aug;153(4):1577–1586. PMID: 20562230; PMCPCMC2923913.
- [60] Zolman BK, Silva ID, Bartel B. The *Arabidopsis pxa1* mutant is defective in an ATP-binding cassette transporter-like protein required for peroxisomal fatty acid β -oxidation. *Plant Physiol*. 2001;127(3):1266–1278.
- [61] Hofius D, Schultz-Larsen T, Joensen J, et al. Autophagic components contribute to hypersensitive cell death in *Arabidopsis*. *Cell*. 2009 May 15;137(4):773–783. PMID: 19450522.
- [62] Matsushita M, Suzuki NN, Obara K, et al. Structure of Atg5•Atg16, a complex essential for autophagy. *J Biol Chem*. 2007 Mar 2;282(9):6763–6772. PMID: 17192262.
- [63] Hu TT, Pattyn P, Bakker EG, et al. The *Arabidopsis lyrata* genome sequence and the basis of rapid genome size change. *Nat Genet*. 2011 May;43(5):476–481. PMID: 21478890; PMCPCMC3083492.
- [64] Yoshimoto K, Jikumaru Y, Kamiya Y, et al. Autophagy negatively regulates cell death by controlling NPR1-dependent salicylic acid signaling during senescence and the innate immune response in *Arabidopsis*. *Plant Cell*. 2009 Sep;21(9):2914–2927. PMID: 19773385; PMC2768913.
- [65] Lenz HD, Haller E, Melzer E, et al. Autophagy differentially controls plant basal immunity to biotrophic and necrotrophic pathogens. *Plant J*. 2011 Jun;66(5):818–830. PMID: 21332848.
- [66] Zolman BK, Bartel B. An *Arabidopsis* indole-3-butyric acid-response mutant defective in PEROXIN6, an apparent ATPase implicated in peroxisomal function. *Proc Natl Acad Sci USA*. 2004 Feb 10;101(6):1786–1791. PMID: 14745029; PMCPCMC341854.
- [67] Deosaran E, Larsen KB, Hua R, et al. NBR1 acts as an autophagy receptor for peroxisomes. *J Cell Sci*. 2013 Feb 15;126(Pt 4):939–952. PMID: WOS:000317585300008.
- [68] Rodríguez MC, Wawrzynska A, Sirko A. Intronic T-DNA insertion in *Arabidopsis NBR1* conditionally affects wild-type transcript level. *Plant Signal Behav*. 2014;9(12):e975659. PMID: 25482782; PMCPCMC4622546
- [69] Chehab EW, Kim S, Savchenko T, et al. Intronic T-DNA insertion renders *Arabidopsis opr3* a conditional jasmonic acid-producing mutant. *Plant Physiol*. 2011 Jun;156(2):770–778. PMID: 21487047; PMCPCMC3177274.
- [70] Hackenberg T, Juul T, Auzina A, et al. Catalase and *NO CATALASE ACTIVITY1* promote autophagy-dependent cell death in *Arabidopsis*. *Plant Cell*. 2013 Nov;25(11):4616–4626. PMID: WOS:000329174400025.
- [71] Juul T, Malolepszy A, Dybkaer K, et al. The in vivo toxicity of hydroxyurea depends on its direct target catalase. *J Biol Chem*. 2010 Jul 9;285(28):21411–21415. PMID: 20452979; PMCPCMC2898382.
- [72] Kulich I, Pečenková T, Sekereš J, et al. *Arabidopsis* exocyst subcomplex containing subunit EXO70B1 is involved in autophagy-related transport to the vacuole. *Traffic*. 2013;14(11):1155–1165.
- [73] Ono Y, Wada S, Izumi M, et al. Evidence for contribution of autophagy to Rubisco degradation during leaf senescence in *Arabidopsis thaliana*. *Plant Cell Environ*. 2013 Jun;36(6):1147–1159. PMID: 23215962.
- [74] Hong SB, Kim B-W, Lee K-E, et al. Insights into noncanonical E1 enzyme activation from the structure of autophagic E1 Atg7 with Atg8. *Nat Struct Mol Biol*. 2011 Dec;18(12):1323–1330. PMID: WOS:000298011600017.
- [75] Yamazaki-Sato H, Tanida I, Ueno T, et al. The carboxyl terminal 17 amino acids within Apg7 are essential for Apg8 lipidation, but not for Apg12 conjugation. *FEBS Lett*. 2003;551(1–3):71–77.
- [76] Noda NN, Satoo K, Fujioka Y, et al. Structural basis of Atg8 activation by a homodimeric E1, Atg7. *Mol Cell*. 2011 Nov 4;44(3):462–475. PMID: 22055191.
- [77] Taherbhoy AM, Tait SW, Kaiser SE, et al. Atg8 transfer from Atg7 to Atg3: a distinctive E1-E2 architecture and mechanism in the autophagy pathway. *Mol Cell*. 2011 Nov 4;44(3):451–461. PMID: 22055190; PMCPCMC3277881.
- [78] Farré JC, Burkenroad A, Burnett SF, et al. Phosphorylation of mitophagy and pexophagy receptors coordinates their interaction with Atg8 and Atg11. *EMBO Rep*. 2013;14(5):441–449.
- [79] Jaillais Y, Fobis-Loisy I, Miegé C, et al. AtSNX1 defines an endosome for auxin-carrier trafficking in *Arabidopsis*. *Nature*. 2006 Sep 7;443(7107):106–109. PMID: 16936718.
- [80] Qin G, Ma Z, Zhang L, et al. *Arabidopsis AtBECLIN 1/AtAtg6/AtVps30* is essential for pollen germination and plant development. *Cell Res*. 2007 Mar;17(3):249–263. PMID: WOS:000246128100007.
- [81] Fujiki Y, Yoshimoto K, Ohsumi Y. An *Arabidopsis* homolog of yeast *ATG6/VPS30* is essential for pollen germination. *Plant Physiol*. 2007 Mar;143(3):1132–1139. PMID: WOS:000244757700007
- [82] Shin KD, Lee HN, Chung T. A revised assay for monitoring autophagic flux in *Arabidopsis thaliana* reveals involvement of *AUTOPHAGY-RELATED9* in autophagy. *Mol Cells*. 2014 May;37(5):399. PMID: 24805779; PMCPCMC4044311
- [83] Floyd BE, Morriss SC, MacIntosh GC, et al. Evidence for autophagy-dependent pathways of rRNA turnover in *Arabidopsis*. *Autophagy*. 2015;11(12):2199–2212. PMID: 26735434; PMCPCMC4835196.
- [84] Hanaoka H, Noda T, Shirano Y, et al. Leaf senescence and starvation-induced chlorosis are accelerated by the disruption of an *Arabidopsis* autophagy gene. *Plant Physiol*. 2002 Jul;129(3):1181–1193. PMID: 12114572; PMCPCMC166512.
- [85] Woo J, Park E, Dinesh-Kumar S. Differential processing of *Arabidopsis* ubiquitin-like Atg8 autophagy proteins by Atg4 cysteine proteases. *Proc Natl Acad Sci USA*. 2014 Jan 14;111(2):863–868. PMID: 24379391; PMCPCMC3896200.
- [86] Farré J-C, Manjithaya R, Mathewson RD, et al. PpAtg30 tags peroxisomes for turnover by selective autophagy. *Dev Cell*. 2008 Mar;14(3):365–376. PMID: 18331717; PMCPCMC3763908.
- [87] Motley AM, Nuttall JM, Hettema EH. Pex3-anchored Atg36 tags peroxisomes for degradation in *Saccharomyces cerevisiae*. *Embo J*. 2012 Jun 29;31(13):2852–2868. PMID: 22643220; PMCPCMC3395097.
- [88] Lin Y-L, Sung S-C, Tsai H-L, et al. The defective proteasome but not substrate recognition function is responsible for the null phenotypes of the *Arabidopsis* proteasome subunit RPN10. *Plant Cell*. 2011;23(7):2754–2773.
- [89] Kaur N, Zhao Q, Xie Q, et al. *Arabidopsis* RING peroxins are E3 ubiquitin ligases that interact with two homologous ubiquitin receptor proteins. *J Integr Plant Biol*. 2013 Jan;55(1):108–120. PMID: WOS:000318600300001.
- [90] Farmer LM, Book AJ, Lee K-H, et al. The RAD23 family provides an essential connection between the 26S proteasome and ubiquitylated proteins in *Arabidopsis*. *Plant Cell*. 2010 Jan;22(1):124–142. PMID: WOS:000275926100012.
- [91] Kao Y-T, Gonzalez KL, Bartel B. Peroxisome function, biogenesis, and dynamics in plants. *Plant Physiol*. 2018 Jan;176(1):162–177. PMID: 29021223; PMCPCMC5761812
- [92] Zhang J, Tripathi DN, Jing J, et al. ATM functions at the peroxisome to induce pexophagy in response to ROS. *Nat Cell Biol*. 2015 Oct;17(10):1259–1269. PMID: WOS:000362213500006.

- [93] Platta HW, El Magraoui F, Bäumer BE, et al. Pex2 and Pex12 function as protein-ubiquitin ligases in peroxisomal protein import. *Mol Cell Biol.* 2009 Oct 15;29(20):5505–5516. PMID: WOS:000270271100010.
- [94] Zientara-Rytter K, Ozeki K, Nazarko TY, et al. Pex3 and Atg37 compete to regulate the interaction between the pexophagy receptor, Atg30, and the Hrr25 kinase. *Autophagy.* 2018;14(3):368–384. PMID: 29260977; PMC5915033.
- [95] Nazarko TY, Ozeki K, Till A, et al. Peroxisomal Atg37 binds Atg30 or palmitoyl-CoA to regulate phagophore formation during pexophagy. *J Cell Biol.* 2014 Feb 17;204(4):541–557. PMID: 24535825; PMC3926955.
- [96] Burnett SF, Farré J-C, Nazarko TY, et al. Peroxisomal Pex3 activates selective autophagy of peroxisomes via interaction with the pexophagy receptor Atg30. *J Biol Chem.* 2015 Mar 27;290(13):8623–8631. PMID: 25694426; PMCPCMC4375511.
- [97] Yamashita S-I, Abe K, Tatemichi Y, et al. The membrane peroxin PEX3 induces peroxisome-ubiquitination-linked pexophagy. *Autophagy.* 2014 Sep;10(9):1549–1564. PMID: 25007327; PMCPCMC4206534.
- [98] Rinaldi MA, Fleming WA, Gonzalez KL, et al. The PEX1 ATPase stabilizes PEX6 and plays essential roles in Arabidopsis peroxisome biology. *Plant Physiol.* 2017;174:2231–2247.
- [99] Gonzalez KL, Ratzel SE, Burks KH, et al. A *pex1* missense mutation improves peroxisome function in a subset of *Arabidopsis pex6* mutants without restoring PEX5 recycling. *Proc Natl Acad Sci USA.* 2018 Apr 3;115(14):E3163–E3172. PMID: WOS:000429012500014.
- [100] Nuttall JM, Motley AM, Hettema EH. Deficiency of the exportomer components Pex1, Pex6, and Pex15 causes enhanced pexophagy in *Saccharomyces cerevisiae*. *Autophagy.* 2014 May;10(5):835–845. PMID: 24657987; PMCPCMC5119063
- [101] Law KB, Bronte-Tinkew D, Di Pietro E, et al. The peroxisomal AAA ATPase complex prevents pexophagy and development of peroxisome biogenesis disorders. *Autophagy.* 2017 May 4;13(5):868–884. PMID: 28521612; PMCPCMC5446072.
- [102] Woodward AW, Bartel B. The *Arabidopsis* peroxisomal targeting signal type 2 receptor PEX7 is necessary for peroxisome function and dependent on PEX5. *Mol Biol Cell.* 2005 Feb;16(2):573–583. PMID: 15548601; PMC545895
- [103] Earley KW, Haag JR, Pontes O, et al. Gateway-compatible vectors for plant functional genomics and proteomics. *Plant J.* 2006 Feb;45(4):616–629. PMID: 16441352.
- [104] Koncz C, Schell J. The promoter of T L-DNA gene 5 controls the tissue-specific expression of chimaeric genes carried by a novel type of *Agrobacterium* binary vector. *Mol Gen Genet.* 1986;204(3):383–396.
- [105] Clough SJ, Bent AF. Floral dip: a simplified method for *Agrobacterium*-mediated transformation of *Arabidopsis thaliana*. *Plant J.* 1998 Dec;16(6):735–743. PMID: 10069079
- [106] Haughn GW, Somerville C. Sulfonylurea-resistant mutants of *Arabidopsis thaliana*. *Mol Gen Genet.* 1986;204(3):430–434. PMID: WOS:A1986D929100010
- [107] Stasinopoulos TC, Hangarter RP. Preventing photochemistry in culture media by long-pass light filters alters growth of cultured tissues. *Plant Physiol.* 1990 Aug;93(4):1365–1369. PMID: 16667626; PMCPCMC1062681
- [108] Neff MM, Turk E, Kalishman M. Web-based primer design for single nucleotide polymorphism analysis. *Trends Genet.* 2002 Dec;18(12):613–615. PMID: 12446140
- [109] Thole JM, Beisner ER, Liu J, et al. Abscisic acid regulates root elongation through the activities of auxin and ethylene in *Arabidopsis thaliana*. *G3: Genes Genomes Genetics.* 2014 Jul 1;4(7):1259–1274. PMID: WOS:000339326600008.
- [110] Li H, Handsaker B, Wysoker A, et al. The sequence alignment/map format and SAMtools. *Bioinformatics.* 2009 Aug 15;25(16):2078–2079. PMID: 19505943; PMCPCMC2723002.
- [111] Cingolani P, Platts A, Wang LL, et al. A program for annotating and predicting the effects of single nucleotide polymorphisms, SnpEff: sNPs in the genome of *Drosophila melanogaster* strain w1118; iso-2; iso-3. *Fly (Austin).* 2012 Apr-Jun;6(2):80–92. PMID: 22728672; PMCPCMC3679285.
- [112] Maeshima M, Yokoi H, Asahi T. Evidence for no proteolytic processing during transport of isocitrate lyase into glyoxysomes in castor bean endosperm. *Plant Cell Physiol.* 1988 Mar;29(2):381–384. PMID: WOS:A1988M630000025
- [113] Olsen LJ, Ettinger WF, Damsz B, et al. Targeting of glyoxysomal proteins to peroxisomes in leaves and roots of a higher plant. *Plant Cell.* 1993 Aug;5(8):941–952. PMID: 8400872; PMCPCMC160329.
- [114] Lingard MJ, Monroe-Augustus M, Bartel B. Peroxisome-associated matrix protein degradation in *Arabidopsis*. *Proc Natl Acad Sci USA.* 2009 Mar 17;106(11):4561–4566. PMID: 19246395; PMC2657447.
- [115] Pracharoenwattana I, Cornah JE, Smith SM. *Arabidopsis* peroxisomal malate dehydrogenase functions in β -oxidation but not in the glyoxylate cycle. *Plant J.* 2007;50(3):381–390.